

Review

Digital Elevation Models of Rockfalls and Landslides: A Review and Meta-Analysis

Maria P. Kakavas and Konstantinos G. Nikolakopoulos * 

Division of Applied Geology and Geophysics, Department of Geology, University of Patras, 26504 Patras, Greece; kakavamaria@upatras.gr

* Correspondence: knikolakop@upatras.gr; Tel.: +30-2610997592

Abstract: The scope of this paper is to summarize previous research pertaining to the use of digital elevation models (DEMs) and digital terrain models (DTMs) in the study of rockfalls and landslides. Research from 1983 to 2020 was surveyed in order to understand how the spatial resolution of DEMs and DTMs affects landslide detection, validation, and mapping. Another major question examined was the relationship between the DEM resolution and the extent of the rockfall or landslide event. It emerged from the study that, for landslides, the majority of researchers used DEMs with a spatial resolution of between 10 m and 30 m, while for rockfalls, they used DEMs with a spatial resolution of between 5 m and 20 m. We concluded that DEMs with a very high resolution (less than 5 m) are suitable for local-scale occurrences, while medium-resolution (from 20 m to 30 m) DEMs are suitable for regional-scale events. High resolution is associated with high accuracy and detailed structural characteristics, while medium accuracy better illustrates the topographic features. A low pixel size (more than 90 m) is not recommended for this type of research. Susceptibility maps, inventory maps, hazard risk zones, and vulnerability assessments are some of the main tools used in landslide/rockfall investigations, and topographic indexes, methods, models, and software optimize the reliability of the results. All of these parameters are closely related to DEMs and DTMs as the cell size affects the credibility of the final outcome.

Keywords: landslides; rockfalls; DEM; DTM; spatial resolution



Citation: Kakavas, M.P.; Nikolakopoulos, K.G. Digital Elevation Models of Rockfalls and Landslides: A Review and Meta-Analysis. *Geosciences* **2021**, *11*, 256. <https://doi.org/10.3390/geosciences11060256>

Academic Editors:
Hans-Balder Havenith and
Jesus Martinez-Frias

Received: 8 April 2021
Accepted: 17 May 2021
Published: 14 June 2021

Publisher's Note: MDPI stays neutral with regard to jurisdictional claims in published maps and institutional affiliations.



Copyright: © 2021 by the authors. Licensee MDPI, Basel, Switzerland. This article is an open access article distributed under the terms and conditions of the Creative Commons Attribution (CC BY) license (<https://creativecommons.org/licenses/by/4.0/>).

1. Introduction

In the last four decades, digital terrain models (DTMs) and digital elevation models (DEMs) have been introduced to research on landslides and rockfalls. DTMs are defined as “digital representations of variables relating to a topographic surface, namely: digital elevation models (DEMs), digital models of gradient (G), aspect (A), horizontal (Kh) and vertical (Kv) land surface curvatures as well as other topographic attributes” [1], while a DEM is a generic term “covering digital topographic data in all its various forms as well as the method for interpreting implicitly of the elevations between observations” [2].

One of the first surveys was performed in 1983 and achieved a morphometric analysis of open rock basins in rockfalls in Canada by means of digital elevation data in combination with aerial data and stereoplottling [3]. In 1987, DTMs were developed from the contour lines of topographic maps for mapping snow, avalanche, and rockfall hazard zones in Norway [4]. Starting points and run-out distances were illustrated and calculated through these models. The importance of grid analysis was outlined, as it offers much more detailed terrain characteristics in lieu of x, y, and z values.

The introduction of spatial resolution started in the early 1990s. In 1993, a DEM with a spatial resolution of 24 m was constructed with the ultimate goal of analyzing potential landslides [5]. Five years later, the effect of a 10 m DEM for the evaluation of shallow landslides was analyzed [6]. DEMs of different resolutions have been used as inputs in rockfall software, with the accuracy of the export data being in line with the chosen resolution [7].

At the beginning of the 21st century, the necessity of high-resolution DEMs in geomorphological analysis for landslide transport was underlined [8]. The opportunity to use DEMs with multiple resolutions to study large-scale landslides in areas where an in situ observation would not be possible was outlined [9]. A few years later, it was reported that DEMs with a higher pixel size could detect the internal characteristics of landslides, which could not be measured through a field survey [10].

In the last decade, the calculation of terrain variation and sharper slope angles through high-resolution models was studied [11]. Additionally, high-resolution DEMs offer better capturing of morphology and accuracy in velocities than low-resolution DEMs [12]. DEMs with a higher accuracy export more detailed outcomes for the majority of landslide factors, but this is not the rule for every analysis [13].

Over the years, the resolution of DEMs and DTMs has increased, and many more researchers have tried to find an appropriate resolution for the scope of their study. This makes sense, as through these digital models, topographic indexes, methods, and software are applied, calculated, and illustrated. A literature analysis of DEMs/DTMs' effect on rockfall and landslide indexes, parameters, factors, and software is the aim of this study.

2. Topographic Indexes

The topographic parameters derived from digital models play a crucial role in susceptibility mapping. Slope (angle, gradient, aspect) (SL) and curvature are extracted from DEMs and DTMs and offer important information regarding the stability of an area [6,9,10,12–41]. It was observed that slope angles in the field are larger than those produced by 0.5 m DEMs, and that in situ observation focuses on steep slope measurements, in contrast with DEMs [42]. It was also proven that DTMs derived from large-scale topographic maps led to more accurate outcomes, as the opposite (DTM from small-scale maps) led to a flattening of the topography of steeper slopes and a loss of crucial information [43]. On the other hand, sharper slope angles can be calculated by models of high resolution [11], as smaller grid sizes are more appropriate for providing detailed information on slope parameters [44]. DEMs' accuracy affects lateral dispersion capture, as the lateral dispersion from a finer DEM increases with a slope inclination of 45° [45].

Digital models are also attached with a topographic position index (TPI) [17,18,20,29,30,46,47], topographic wetness index (TWI) [6,7,13,17,20,26,29,30,33–37,41,46–50], topographic roughness index (TRI) [13,17,18,20,21,23,29,30,33,36], compound topographic index (CTI) [21,32,40,51], sediment transport index (STI) [13,17,32,35,36,47], stream power index (SPI) [13,17,20,21,29,30,32–37,40,41,50,51], and normalized difference vegetation index (NDVI) [13,21,22,26,28,35,36,38,52–58]. An unmanned aerial vehicle (UAV) method for vegetation parameters was proposed, as it removes vegetation, offers high-resolution images, and is inexpensive [59]. DEMs with a high-resolution extract detailed information on the topography and, consequently, offer more reliable evaluation of the factors [18].

The frequency of the measurement of topographic indexes for landslide/rockfall studies is shown in the following pie chart, and is based on this literature review (Figure 1). According to the pie chart, the majority of the research focused on slope calculation at a rate of 30%. This was also confirmed by a previous study [17] in which it was underlined that the dominant factor for rockfall/landslide mapping was the slope angle, whose measurement was most affected by DEMs' resolution. The factor of TWI was used at a rate of 17%, and NDVI and SPI at a rate of 14%. This is logical, as the wetness, vegetation, and stream power affect rockslide events. The indexes of TPI and TRI are in moderate use at rates of 7% and 8%, respectively, while STI and CTI are in low preference at rates of 6% and 4%, respectively.

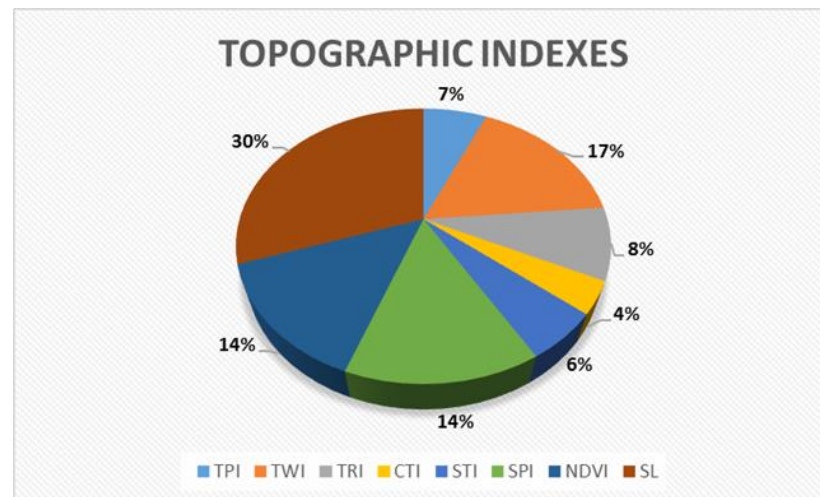


Figure 1. Pie chart illustrating the most and least frequently calculated landslide indexes.

3. Methods

Landslide susceptibility maps, hazard risk zones, and vulnerability classification are some of the major goals in landslide/rockfall assessment. Two parameters are essential for reaching these goals. The first is the DEM with the appropriate resolution based on the offered data, while the second is related to the selected method. These two parameters are in conjunction with each other. For this study, a plethora of articles were selected from Scopus, Google Scholar, and Research Gate. The above selection was made according to their level of relationship with the area of interest, the chronology of the study, and the number of citations. The main subject is the spatial resolution of DEMs in each method. The gathered data were input into an Excel program and diagrams were extracted, showing the most and least used methods.

An analytical hierarchy process (AHP) [20,54,60–62], the probabilistic likelihood ratio (PLR) [20,60,61,63], a fuzzy method (FM) [31,36,56,60], and the hybrid likelihood approach (HL) [60,64] have been widely used for landslide susceptibility mapping, and the influence of DEMs has been described. Many researchers have applied more than one method in their research, aiming to compare the outcomes and decide on the most reliable method [20,60,63].

In addition, the neural network method contributes to landslide studies. Triangular irregular networks (TIN) [7,10,61,65,66] are interpolation techniques that lead to DEM production and, as a consequence, to rockfall investigation. On the other hand, artificial neural networks (ANN) [18,19,21,39,50,58,63,67] lead to direct landslide susceptibility map generation by exploiting topographic databases, and are indirectly connected with DEMs. One more neural network method is the feedforward back-propagation neural network (FBPNN) [18,33,39,58]. Furthermore, the area under the curve (AUC) model [21,30,33–37,39–41,46,50,58,68–70] and receiver operating characteristic (ROC) model [21,33,34,37,39–41,56,58,68] have been widely used in order to validate the analysis and mapping techniques. The first is a quantitative measure of prediction, and the second is a depiction of sensitivity.

Landslide/rockfall surveys are also achieved with methods such as ground control points collection (GPS) [12,28,31,39,49,52,56,71–80], aerial photo interpretation (photogrammetry) (API) [7,9,10,14,16,28–32,37,40,44,47,49,50,56–59,61,66,67,71,72,76,79,81–95], and terrestrial photo interpretation (TPI) [71,90], in conjunction with field observations. These methods offer investigations either of local-scale events or at a regional level, where in situ observation is not always possible.

In addition to the traditional monitoring methods, satellite radar interferometry (InSAR) [12,48,74,77,79,87,96], satellite imagery (SI) [10,12,14,19,27,28,30,36,38,47,50,52,56–59,62,63,70,77,79,88,92–97], aerial laser scanning (ALS) [12,65,71,73,75], terrestrial laser

scanning (TLS) [59,64,65,67,71,73,98,99], and light detection and ranging (LiDAR) [10,18,21,23,24,26,59,60,64,65,72,73,78,83,100–104] techniques have been used for landslide detection, evaluation, and validation. These techniques contribute to the surveys by producing images that lead to detailed observation or to DEMs generation. The last process is crucial as DEMs at multiple spatial resolution can be created and then, if necessary, to resample in other resolutions.

Mathematical methods such as the kriging method (KM) [61,65,92,98,101,104] or lumped mass method (LM) [24,45,64,66,99,103,105–107] are based on an algorithm and linked with software for the detection of rockfall trajectories. Bivariate methods, such as the use of weights of evidence (WofE) [21,35,38,41,92], the frequency ratio (FR) [21,37,39,41,50,57,58,68,70,108], the certainty factor (CF) [18,47,70], and multivariate methods such as discriminant analysis (DA) [21] and logic regression (LR) [21,30,33,34,41,47,50,58,63,68,85,109], are commonly accepted for landslide susceptibility mapping.

Last but not least, through the matrix (MM) [29,86], random finite element (RFEM) [11,64], and sloping local base level (SLBL) methods [9,42,110], a structural analysis is feasible, while, with the Monte Carlo method (MCM) [24,46,111], an analytical rockfall simulation is possible. The appropriate DEM/DTM as input data, in any type of method, gives key information that ensures a reliable result.

Every model has its pros and cons. The ANN method offers better results than the LR and the FR [58]. Generally, neural network methods offer better results than the LR method, especially in high and very high zones [33]. The ANN model correctly estimates landslides' potential areas but is not suitable for extracting detailed landslide susceptibility values [39]. By contrast, the LR method gave better results than the evidential belief function and support vector machine methods [30]. According to previous research [29], the matrix method offers the most accurate susceptibility map as the distribution of slope movements explained by this method. Maps' credibility can be evaluated through AUC and ROC methods [41]. The selection of the appropriate models is also in conjunction with the morphology of the area of interest. The most reliable approach for mountainous areas is the weights of evidence (WofE) method, in contrast with the statistical index and index of entropy (IOE) methods [35]. It has proven that the FR method offered more credible landslide mapping than the WofE and LR and that the LR led to less accurate map production [41]. LiDAR DEM offers high accuracies in the HL and FM methods and moderate accuracy in the AHP, while ASTER GDEM and NED (National Elevation Dataset) DEMs range from low to moderate accuracy in these methods [60].

The frequency of the methods used for landslide/rockfall studies is shown in the following diagram and is based on this literature review (Figure 2). According to this diagram, most researchers preferred photogrammetric methods, API, SI, LiDAR, and GPS at a rate from 8% to 18%, which is logical as these offer detailed information on the topography as well as the opportunity to create new DEMs according to the demands of the respective research. The network methods (ANN, TIN, and FBPNN) have been sparingly used at a rate from 1.7% to 3.4%, with the ANN method producing a larger rate. The AUC and ROC models gave rates of 6.5% and 4%, respectively, and via them an evaluation of the credibility of the final maps was possible. The scanning methods, ALS, TLS, and InSAR, were moderately used at a rate of 3%. Additionally, the APH, KM, LM, WofE, FR, and LR methods were of moderate preference and many researchers used more than one in their study, aiming to compare the results and determine which was the most reliable. Of these methods, LR had the highest rate (4%). The rest of the models, PLR, FM, HL, TPI, CF, MM, RFEM, SLBL, and MCM, were used at a rate of less than 1.5%. This small percentage of preference may be due to model restrictions, which lead to implementation difficulties, or these models may be more appropriate for other types of study.

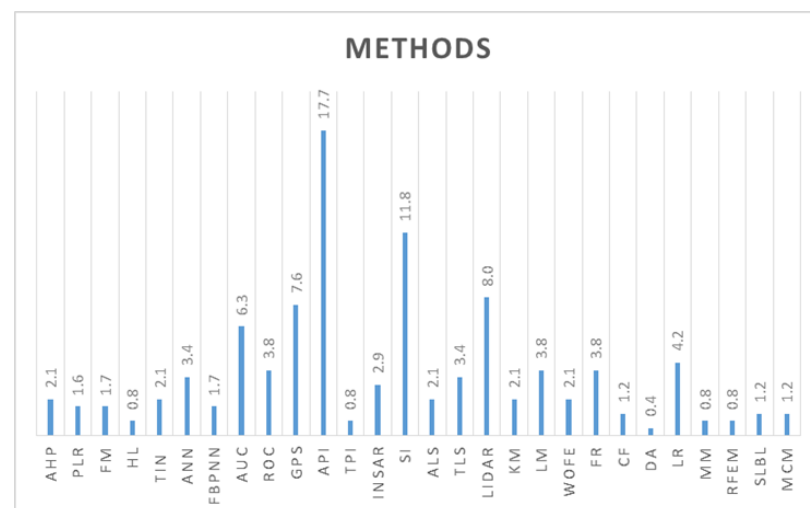


Figure 2. Diagram illustrating the most and least frequently used methods.

4. Software

Numerous types of software have been developed in order to produce 2D or 3D rockfall trajectory simulations through the use of DEMs/DTMs. Nowadays, the precision of trajectories' calculation is at a very high level due to advanced numerical simulations [112]. ROCKFALL software accomplishes 2D rockfall animation by calculating the kinetic energy, velocity, and bounce-height along a specified slope profile [14,104,113]. DEMs are useful tools for motion simulation, via Rockyfor3D [114,115] and GeoRock 2D and 3D [99,116,117] software, as they produce information on rockfall trajectories.

RAMMS 3D software computes runout trajectories and rockfall motion through the input DEMs and leads to more accurate results if the upload DEM is of high resolution [118]. In RAMMS software, the cell size does not affect the simulation outcomes in flattened areas but does in rough areas; for that reason, the use of finer resolution on this occasion is consistent [118]. Another type of software contingent on DEMs' resolution is SINMAP, which focuses on the stability of a slope through grid-based data structures [7,102,119]. MATTEROCKING software uses DEMs to obtain the characteristics of discontinuities and detect rock slope instabilities [109,110,120,121].

STONE software offers a 3D simulation and evaluation of rockfall trajectories that is based on a lumped mass algorithm [45,64,66,82,89,99,105,106,122]. DEMs are required as input data and the advantage of this software is that the algorithm does not have spatial resolution limitations [107]. A similar program is the 3D HY-STONE simulation code, which offers a high-resolution 3D slope morphology illustration [64,82]. HY-STONE was applied and we observed that DEMs with lower accuracy led to a longer runout simulation [64]. The ROTOMAP 3D program is also based on a lumped mass algorithm, which requires a DEM to determine the block parameters [98,99,123].

COLPTOP3D is a 3D software in which DEMs are uploaded and the orientation of each single cell of the DEM is computed [16,42,110,124]. The histograms of slope angle, topographic analysis in 3D, residual and regional topography, and kinematic tests are some parameters that can be extracted from the DEM cell and integrated in the aforementioned program [16]. CONEFALL software computes velocities and kinetic energies in conjunction with the runout areas and, with the aid of DEMs and DTMs, extracts rockfall activity details [101,102,109,110,125,126]. ILWIS software is suitable for general-scale rockfall events to calculate the velocities and distances of debris by developing a neighborhood analysis from counting close pixels through DTMs [43,49,127].

The frequency of the use of different software in landslide/rockfall investigation is shown in the following pie chart and is based on this literature review (Figure 3). According to this pie chart, most researchers preferred, at a rate of 25%, the 3D STONE software. This may be due to the lack of resolution restrictions, while HY-STONE software (which

is similar to 3D STONE) was preferred at a rate of 5%. The second most commonly used software was CONEFALL, at a percentage of 17%, and the third was COLPTOP, at 11%, with both types of software offering detailed kinetic information on rockslides. MATTEROCKING was used by 8%, while ROCFALL, ILWIS, ROTOMAP, and SINMAP software were present in the studies but not as frequently as the above (8%). The less used software types were RAMMS, ROCKYFOR3D, and GEOROCK 2D and 3D, which analyze rockfall trajectories and were chosen at a rate of 3%. These three programs are newer than the others and have been gaining momentum in recent years. The low rate (3%) can be explained by this study containing data from a 30+-year period; hence, the older software types have already been used by a higher number of researchers.

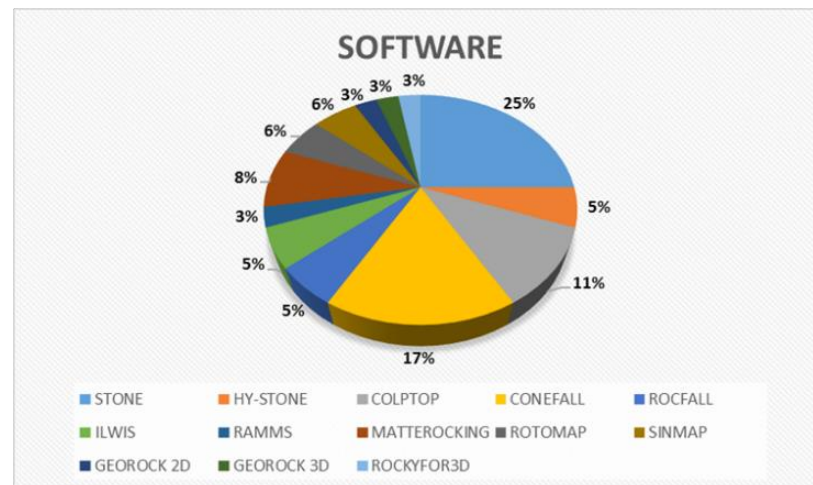


Figure 3. Pie chart illustrating the most and least frequently used software.

5. Spatial Resolution

5.1. The Effect of Digital Elevation Model (DEM) Resolution on Landslides

Digital models have been widely used for landslide investigation. Multiple spatial resolutions have been used, over the years, by many researchers, aiming to obtain accurate results and illustrate reliable risk assessment zones and landslide susceptibility maps. The choice of DEM/DTM resolution depends on the landslide scale, which DEM/DTM is available, the cost, the time of acquisition, and the country where the survey was conducted, as every country has its own DEM/DTM, which is usually of a smaller pixel size than global DEMs. When a resolution is not appropriate, resampling [22,60,102] or degrading [102] in a new resolution is a solution that many researchers have benefited from. A literature review based on DEM/DTM resolution is given in the following pages, in chronological order:

Carrara et al. (1991) applied an interpretation method for landslide hazard evaluation [128]. A 25 m resolution DTM, derived from a 1:25,000 scale topographic map, aerial photographs, field surveys, and rainfall data collection, contributed to the cartography of a drainage basin in Central Italy and to the demonstration of landslide-triggering mechanisms.

Gao (1993) constructed a DEM with 24 m spatial resolution, with the ultimate goal of analyzing potential landslides in the mountains of Virginia, USA [5]. The distribution of landslides' probability, combined with the slope orientation, elevation, slope gradient, and shape, was examined with the aid of the created DEM. He also utilized aerial photographs, taken in 1971, to acquire topographic information.

Borga et al. (1998) analyzed the effect of a 10 m DEM derived from a topographic map at a scale of 1:1000 and applied two hydrological models (TOPMODEL and WODITEM) for the evaluation of shallow landslides [6]. They took into account multiple parameters such as topography, slope instability, drainage system, runoff, etc. in order to estimate the stable and unstable areas in Cordon catchment in Italy. The results from the model computation and the in situ observations were captured and correlated.

Pack et al. (1998) used SINMAP software to categorize stable and unstable slope zones of Vancouver Island [7]. The groundwater conditions, the distance from the catchment area, and the water pressure affect the triggering of a landslide. Consequently, these water parameters were input in the aforementioned software to achieve a reliable inventory map. A DEM with a 10 m grid was also input in the program and they observed that the resolution of the input DEM was correlated with the results' accuracy.

Guzzetti et al. (1999) achieved a landslide methodology cartography based on previous research in the areas of interest in Central Italy [88]. Grid cells, terrain units, unique condition units, slope units, and topographic units are some of the required mapping units in landslide hazard evaluation. They concluded that the mapping unit's selection was influenced more by the chosen software than by the geological data. In this study, a DTM with 25 m resolution was input in the used software.

Agliardi et al. (2001) focused on the kinetic of slope gravitational deformation and landslide-triggering mechanisms in Italy [91]. Aerial photos were interpreted and a 10 m grid DEM derived from a 1:10,000 topographic map was used to investigate geomorphological settings, tectonic lineaments, gravitational morphostructures, and kinematic activity. The slope evolution was illustrated via a 2D numerical model.

Vanacker et al. (2003) presented the effects of deforestation on the instability of slopes and, by extension, on landslide events [49]. They calculated and evaluated multiple parameters (hydrological, flow accumulation, runoffs, slope movements, land uses, etc.) with the use of a 5 m-resolution DEM, aerial photographs, GPS points, ILWIS software, TOPOG mode, and a series of in situ observations. They divided the area of interest, in the Ecuadorian Andes, into landslide and no-landslide areas and compared the results of safety factors in both areas.

Jaboyedoff et al. (2004), in the second part of their research, investigated the base level of the slope in Randa's rockfall, in Switzerland [9]. DEMs enabled the illustration of slope movements and the calculation of the volume of rock. With the use of DEMs, an abundance of information was gained in a minimum time, with limited expenses, and at a large scale. The assessment of landslide hazards was accomplished with DEM pixel processing. The typical Swiss DEM (Swisstopo) with a spatial resolution of 25 m and aerial photographs indicated potentially unstable slopes.

Gunther et al. (2004) observed slope stability and instability in Germany [76]. Geotechnical, hydrological, and meteorological data contributed to the susceptibility mapping of slopes by exploiting a DSM and a 5 m cell size DEM (ATKIS DGM5). Each pixel was calculated, analyzed, and integrated into raster and vector environments.

Pesci et al. (2004) observed the monitoring of landslides in Emilia-Romagna, Italy, via the construction of three DEMs [71]. One DEM was extracted by GPS points with 1 m resolution, the second by an airborne and terrestrial laser scanning technique with the same resolution, and the third by aerial photogrammetry with 0.3 m accuracy. More precisely, GPS techniques offer high accuracy with low cost. Digital photogrammetry expands the time, while the accuracy depends on the scale of the aerial photos, where the vegetation is taken into account. Terrestrial laser scanning is low cost and low accuracy, while aerial photogrammetry offers a high level of both. In the last technique, 3D RiScan software was used.

Lee et al. (2004) estimated the role of pixel size of DEMs in landslide susceptibility mapping. DEMs with 5 m, 10 m, 30 m, 100 m, and 200 m cell size, 40 aerial photographs, and numerous field surveys were performed for the computation of multiple landslide factors like the frequency ratio of slope aspect, curvature, soil (type, texture, drainage, material, effective thickness) forest (type, density), timber (diameter, age), lithology, lineament, and land use [108]. The results were satisfactory only from DEMs with a resolution of less than 30 m. In contrast, DEMs with resolutions of 100 m and 200 m gave unsatisfactory results in this type of research.

Nichol et al. (2005) identified landslides via SPOT and IKONOS satellite images [95]. The resolution of the aforementioned images was described as they wanted to achieve a detailed inventory map and the resolution affects the accuracy of the results. In order to

meet their goal, an orthorectification procedure was needed and was achieved through a 5 m pixel size DEM, derived from a contour map.

Yesilnacar et al. (2005) selected a logical regression and a feedforward back-propagation neural network approach to produce landslide susceptibility maps and compare and evaluate these maps according to their topographic indexes [33]. Morphometric and hydrological attributes of the terrain were extracted from a 25 m pixel size DEM derived from a 1:25,000 scale topographic map. They concluded that the neural network method offered better results than the logical regression method, especially in high and very high zones.

Lee et al. (2005) selected a probabilistic approach via a frequency ratio index in order to demonstrate landslide hazard zones in Malaysia [57]. Landsat Thematic Mapper and SPOT HRV satellite images, aerial photographs, and a 10 m DEM from a topographic map extracted useful data for landslide prediction.

Claessens et al. (2005) focused on how DEMs with dissimilar resolutions (10 m, 25 m, 50 m, and 100 m) affect the landslide hazard in shallow forms and the calculation of soil debris reallocation [129]. This reallocation was accomplished with the use of a LAPSUS-LS model, which is correlated with the runoff and the cultivated erosion. They proved that DEMs with a finer grid size better illustrate the topographical and hydrological conditions.

Lee et al. (2006) focused on the creation of a landslide susceptibility map in Korea [63]. Landslides were caused by heavy rainfall, and their study included data analysis and collection via satellite imagery, field survey, Matlab software, and a DEM derived from a topographic map with 10 m resolution. An artificial neural network was incorporated in their landslide analysis and provided valuable information.

Ardizzone et al. (2007) described the influence of rainfall on landslide triggering via 2 m and 10 m pixel size LiDAR DEMs [72]. They collected rainfall data, extracted morphological details, used multiple types of software, and analyzed the exported meteorological, geological, and topographical data. They found that areas with previous landslides were more easily identified from DEMs than the others, and the DEM with the higher resolution offers better mapping of the topography.

Gorsevski et al. (2008) chose a mathematical rough set approach to analyze the geographic characteristics in landslides [32]. Aerial photo interpretation, a 30 m resolution DEM, and multiple topographic indexes led to landslide susceptibility mapping. Additionally, road-related and non-road-related methodologies contributed to the mapping via a fuzzy approach.

Tarolli et al. (2009) pointed out that the morphological scale of an event should be taken into account in the landform recognition process by means of DTMs [100]. DTMs with 1 m, 3 m, 5 m, 10 m, 20 m, and 30 m resolution derived from LiDAR data were applied in the geomorphological parameters' calculation. They found that a finer resolution than 10 m may give more precise landslide information as it better reflects the local conditions.

Jaboyedoff et al. (2009) concentrated their study of landslides on the Frank, in Alberta [42]. Through photogrammetric techniques, orthophotos and DEMs, with 0.5 m spatial resolution, were created with the aim of being uploaded to COLTOP-3D software and extracting each cell's orientation for a further structural analysis. The aforementioned spatial accuracy minimizes the root mean square error and consequently offers more accurate results. Processing of these data leads to the identification of rock failure structures and the characterization of rockslide features. Conclusions extracted from this survey are that the slope angles in the field are larger than those produced from DEMs and that the in situ observation focuses on steep slope measurements in contrast with DEMs.

Kawabata et al. (2009) generated a landslide susceptibility map for unstable areas of Niigata Prefecture, Japan, via the use of two indexes [19]. The first was related to the artificial neural network and the second to two DEMs. These DEMs are ASTER DEM, which was extracted by satellite images with 15 m spatial resolution and 8.6 m root mean square error (RMSE) and a DEM that was produced by the Geographical Survey Institute of Japan with 55 m spatial resolution and 7.2 m RMSE. According to these researchers, this method has 90% accuracy regarding the prediction of possible

future rockfalls. The second DEM covers large-scale occurrences and, thus, results in high-accuracy data due to the fact that this pixel size do not take into account sudden data value changes.

Kasai et al. (2009) utilized a 1 m pixel size LiDAR DEM to analyze factors such as slope angle, eigenvalue ratio, landslide inventory, and data from in situ observations [23]. They recommended this DEM for small-scale events as it can produce fruitful information for possible future landslides that may cause fatalities and the destruction of land. At a large scale, DEMs with lower resolution are more appropriate.

Pradhan et al. (2010) calculated, via the use of a 10 m resolution DEM and satellite and aerial images, 11 landslide factors and then removed the factors that were less influential according to the extracted values [58]. In addition, the three methods, ANN, FR, and LR, were compared and they concluded that ANN offers the most reliable landslide susceptibility results.

Miner et al. (2010) produced DEMs from LiDAR datasets, with 1 m, 2 m, and 5 m pixel size, to achieve landslide recognition around Australia [10]. They determined that the most appropriate pixel size is 5–10 m for landslide feature detection; otherwise, these features could not be detected and identified. On the other hand, DEMs with a higher pixel size (1 m) can detect the internal characteristics of landslides that could not be measured through field observation.

Mancini et al. (2010) applied a logistic regression approach, in the Italian Apennines chain, to extract a landslide susceptibility map [85]. SPSS software and a DEM with a 40 m cell size created from aerial photographs were used. DEM resolution was taken into account as it affects the altitude accuracy, which is one of the main topographic factors and gives key information about morphometric causal factors.

Martha et al. (2010) semi-automatically detected landslides in the Himalayas via spectral, spatial, and morphometric information [28]. Satellite data and a DEM with 10 m resolution, generated from Cartosat-1 data, allowed for object classification and a hazard analysis. The landslides were classified into traditional, shallow traditional, rotational rockslides, and debris flow types.

Pradhan et al. (2010) used a neuro-fuzzy model to analyze landslide conditioning factors and generate susceptibility maps in Malaysia [56]. Aerial photographs, SPOT-5, IKONOS, RADARSAT satellite images, and a DEM with 10 m resolution derived from a topographic map at scale of 1:25,000 led to a landslide inventory map.

McLean (2011) focused her Master's thesis on the investigation of landslide risk assessment in Chamonix, France and southwestern Norway [130]. She took advantage of GTOPO DEM and SRTM DEM, both with 30 m resolution, to calculate parameters such as the slope angle, slope failure, elevation, cohesion, averaging dimensions, etc. She found that the GTOPO DEM extracts less accurate results than SRTM DEM.

Keijesers et al. (2011) elaborated on the calibration and confirmation of landslide prediction with the LAPSUS-LS model [81]. DEMs with 9 m, 27 m, 54 m, and 81 m resolution were uploaded for the measurement of slope, rainfall, land-use, and hence, the stability or instability of a specific area of Taiwan. The percentage of the aforementioned prediction was reduced with the resolution mitigation as DEMs with lower accuracy flatten the topography's roughness.

Gorum et al. (2011) mapped a landslide in Sichuan Province, China, which was triggered by an earthquake [79]. They focused on a series of mechanisms—hydrological, geological, and structural—to describe and prevent future landslides. The analysis was divided into pre-earthquake and post-earthquake periods and was accomplished via a 90 m DEM, derived from a topographic map, and ASTER, ALOS, SPOT-5, IKONOS, and CARTOSAT-1 satellite images of high resolution.

Jaboyedoff et al. (2012) wrote a chapter on rockfall and landslide susceptibility mapping [102]. They created a landslide database, then a stability map, and finally a susceptibility map for two areas in Switzerland. They used, for altitudes lower than 2000 m, a 1 m high-resolution DEM (HRDEM) and a 2 m DEM, both derived from aerial laser

scanning, and, for altitudes higher than 2000 m, a 25 m DEM that was created from a Swiss topographic map with a scale of 1:25,000. They took advantage of many types of software (e.g., Conefall, Ras), models (e.g., Flow-R, Sinmap), and tools (e.g., Histofit) in order to achieve this mapping.

Costanzo et al. (2012) developed two methods to achieve landslide susceptibility mapping in Granada, Spain [29]. The matrix method was applied and stable and unstable areas near Rio Beiro Basin were extracted by taking into account the type of landslide. Topographic and geological factors were obtained with a 10 m resolution DEM. According to them, the matrix method offers the most accurate susceptibility map and the distribution of slope movements is explained by this method.

Ozdemir et al. (2013) measured landslide causative factors, such as topographic, geological, land use, and precipitation, with the aid of a 20 m resolution DEM generated from a topographic map with a scale of 1:25,000 [41]. Then, they collected the causative and dependent factors and implemented them in three different methods, FR, WOE, and LR, in order to create landslide susceptibility maps. The final maps were compared, and the most appropriate method, FR, was revealed.

Martha, et al. (2013) applied the weight of evidence method to demonstrate landslide hazard zones [38]. A DEM with 10 m resolution generated by Cartosat-1 data and satellite images of high resolution were used for topographic indexes' calculation and, furthermore, for susceptibility estimation and validation.

Fenton et al. (2013) concentrated their study on landslide hazard assessment in Chamonix, France [11]. They evaluated the slope angle by using two DEMs: the first was GTOPO with 30 m resolution and the second was SRTM with 3 m resolution. Furthermore, they estimated the slope failure at a critical scale of 10 m. To this end, the Rslope2d program was used since it provides the probability of a slope failure. The resolution of DEMs plays a particular role as terrain variations and sharper slope angles can be calculated by models of high resolution.

Oh et al. (2013) generated a DEM from ASTER satellite imagery with 15 m × 15 m pixel size and approximately 25 m RMSE [52]. The scope was to extract landslide factors (slope, curvature, aspect, etc.) and calculate the landslide susceptibility index in the Boun area of, Korea. Forty black-and-white aerial photographs, taken in 1996–1999, were merged into a mosaic and used for landslide detection and mapping. The researchers concluded that the aforementioned ASTER DEM is appropriate for large-scale occurrences due to its spatial resolution.

Qin et al. (2013) tested two stochastic simulation methods, Monte Carlo and sequential Gaussian, for the observation of uncertainties in landslide mapping due to DEM errors [111]. For this scope, a DEM with 25 m pixel size was introduced and a fuzzy logic-based, logistic regression, and multivariate statistical approach were developed. They found that DEMs with high accuracy lead to more uncertainties, which can be decreased via spatial autocorrelation.

Chen et al. (2013) presented the effect of DEMs' resolution on landslide information exportation and feature characterization [22]. For this scope, a DEM with 10 m spatial resolution and 2.31 m RMSE was used and was resampled to 20 m, 30 m, 60 m, and 90 m resolutions. These accuracies extracted multiple results, the most significant being that accuracies larger than 30 m are more appropriate in areas larger than 5000 m² and that, when the accuracy decreases, the topographic detection of features decreases as well.

Calvello et al. (2013) studied two landslide cases in southern Italy, aiming to illustrate distribution zones [25]. In the first case, with a scale of 1:25,000, a DEM with 25 m resolution was used and in the second case, with a scale of 1:100,000, a SRTM DEM with 95 m was used. They divided the areas of interest into zones, analyzed terrain units, took into account topographic characteristic (but not landslide features), using the DEMs, and created distribution zoning maps.

Chandra et al. (2013) studied landslides in the Himalayas via bivariate and multivariate methods [47]. The bivariate methods included a certainty factor and an index

of entropy model, while the multivariate methods included a logistic regression model. A 20 m resolution DEM was used for the calculation of landslide conditioning factors and, finally, a landslide inventory map was generated.

Fuchs et al. (2014) calculated slopes, cohesion, soil density, elevation, topographic position, wetness index, landslide distribution, and sensitivity analysis with the input of ASTER GDEM (30 m) and GeoElevation DEM (10 m spatial resolution) in order to estimate safety parameters in infinite slope cases [46]. The Monte Carlo simulation method was applied to compute uncertainties in landslides. The two DEMs extracted similar values, except in areas with remarkable relief. The advantage of ASTER GDEM is that it is free of charge, in contrast with GeoElevation DEM.

Dagdelenler et al. (2015) used the seed cell sampling strategy and ROC, AUC, and logical regression methods for susceptibility evaluation [34]. The AUC and ROC of DEMs with 10 m, 12.5 m, and 25 m resolution were calculated and the extracted values compared. They found that a 50 m buffer was the most appropriate distance for seed cell production.

Ciampalini et al. (2015) developed a geodatabase with landslide data from Messina Province [48]. The ultimate goal was to create landslide susceptibility, inventory, hazard, and risk maps in order to prevent future fatalities and infrastructure damage. Auxiliary (analog and digital) and space-borne SAR data were extracted using the IGM DEM (20 m pixel size), orthophotos, and optical images.

Mandal et al. (2015) analyzed, in their book *Semi-quantitative Approaches for Landslide Assessment and Prediction* (specifically in chapter 2), landslides in Shivkhola Watershed, India [27]. A DEM with 25 m resolution, created from a topographic map at a scale of 1:50,000, was used for hypsometric analysis, lithological composition, slope angle, aspect, and curvature calculation. Soil and water characteristics, friction angle (ϕ), and cohesion were also studied.

Huang et al. (2015) interpreted two pairs of ALOS/PALSAR satellite images via InSAR methods in order to create a 15 m grid size DEM and describe Donghekou landslide, in China, before and after the event [96]. In addition, a 90 = 0 m SRTM DEM was used as it disregards flattened areas, which is a restriction of this type of research. A 3D terrain simulation was accomplished and a hazard assessment extracted based on the before and after failure records.

Chang et al. (2016) studied multiple geological and structural factors (slope aspect, slope angle, elevation, curvature, etc.) that contribute to the extraction of landslide susceptibility mapping, aiming at preventing rockfalls near Sihjhong River, Taiwan [18]. They prepared two DEMs, the first a LiDAR DEM with 5 m spatial resolution and the second an ASTER DEM with 30 m spatial resolution, in order to evaluate the aforementioned factors. The results indicated that the DEM with the highest accuracy produced a detailed capture of the topography and, consequently, more reliable values of the factors. The artificial neural network was also taken into account for this mapping.

Pawluszek et al. (2016) developed three strategies to achieve successful landslide susceptibility mapping, via the use of a 5 m \times 5 m cell size DEM, in Roznow Lake, Poland [20]. These strategies included landslide controlling factors (elevation, slope, morphological gradient, aspect, area of solar radiation, roughness, topographic position, wetness index, stream power index, shaded relief), lithological and environmental factors (distance from roads, distance from drainage, land use), and, finally, an analytical hierarchy process.

Mahalingam et al. (2016) processed LiDAR DEM with 10 m resolution for landslide susceptibility and hazard mapping, in Oregon, USA, and concluded that this DEM produces efficient and reliable results [21]. Their study consisted of four stages. The first stage was the preparation (landslide conditioning factors, training and test samples), the second was the analysis (frequency ratio, weights of evidence method, logistic regression, discriminant analysis, artificial neural network, support vector machine), the third was the production and finally, the validation (receiver operating characteristic, area under the curve, histogram analysis).

Ciampalini et al. (2016) used three DEMs in Italian landslide areas: IGM DEM with 20 m spatial resolution and ALS-LiDAR DEM with 1 m and 2 m resolution, to calculate elevation, compare velocities in the orientation of the sharpest slope, evaluate the role of DEMs accuracy, and estimate the landslide activation via the PSInSAR radar [12]. They also included SRTM DEM as it gives the precise position of the GPS points. They proved that high-resolution DEMs offer better capture of morphology and accuracy in velocities than those with low resolution; as a consequence, these are appropriate for landslide mapping and kinematic understanding.

Mahalingam et al. (2016) applied three processing methods, analytical hierarchical, fuzzy logic, and hybrid, to create landslide susceptibility maps in Oregon [60]. Three DEMs, ASTER, LiDAR, and NED, with multiple resolutions (10 m, 30 m, and 50 m), were taken into account in the above methods. The LiDAR DEM offered high accuracy in the hybrid and fuzzy methods and moderate accuracy in the analytical method. The other two DEMs ranged from low to moderate accuracy in all the methods.

Rasyid et al. (2016) achieved landslide susceptibility mapping, in Indonesia, through a frequency ratio and a logistic regression model [68]. The area of interest was trained and validated with the aid of Google Earth image interpretation and with a 30 m cell size ASTER DEM. They concluded that the aforementioned models are appropriate for the prediction of future landslides.

Wang et al. (2016) applied a statistical index and index of entropy models to generate susceptibility maps and evaluated the maps through the area under the curve (AUC) method [69]. A database was generated, and topographic factors were extracted via a 30 m ASTER DEM. The conditioning factors and the data exported from the models were correlated and validated. Both models reported similar outcomes.

Pradhan et al. (2017) applied DEMs with multiple resolutions to study the effect of accuracy on landslide susceptibility mapping [13]. These DEMs were LiDAR DEM (0.5 m, 1 m, 2 m, 3 m, 5 m, 10 m, 20 m, 30 m) and ASTER DEM (30 m spatial resolution). These were introduced for multicollinearity and sensitivity analysis, validation, and comparison. The results showed that DEMs with higher accuracy, for the majority of landslide factors, export more detailed outcomes, but this is not the case for every analysis.

Bianchini et al. (2017) produced a specific risk map using satellite data (SENTINEL-1 band images) and a 20 m pixel size DEM derived from TINITALY DEM [87]. Environmental factors, pre-existing maps, radar, and structure data were taken into account, aiming to develop a susceptibility map with hazard classes, an intensity map with intensity classes, and a vulnerability map with the corresponding classes.

Liu et al. (2018) applied three modeling approaches, statistical index (SI), index of entropy (IOE), and WOE, to achieve landslide hazard zoning in the Shangnan area in China [35]. A 30 m resolution DEM was exploited for topographic values' calculation. The results showed that the most reliable approach for mountainous areas is the WOE method.

Zhu et al. (2018) selected four methods, two presence-only and two presence-absence, to create a landslide inventory map for Gansu Province, China [39]. Predisposing factors were studied with the aid of a 30 m resolution DEM derived from a topographic map scale of 1:50,000 and the stability and instability of the area of interest were extracted. Finally, they proved that the two presence-absence methods give better results than the other methods.

Juliev et al. (2019) presented a landslide risk management in Uzbekistan via three methods [70]. The first was the statistical index, the second was the frequency ratio (both are bivariate approaches), and the third was a certainty factor. Google Earth, GeoEye-1 satellite data, and a 30 m ASTER DEM contributed to the susceptibility mapping.

Dou et al. (2019) studied causative factors such as slope, CTI, SPI, and rainfall data, aiming to illustrate landslide-susceptible areas triggered by heavy rainfalls [40]. The calculation of these factors was accomplished with a 10 m pixel size DEM. The decision tree and

random forest methods contributed to the validation of the export hazard map via the use of the AUC and ROC indexes.

Kakavas et al. (2020) compared six freely available DSMs, aiming to select the most appropriate one for landslide studies [80]. One DSM with high-resolution (5 m) DSM from the Greek Cadastral, three DEMs with medium resolution (30 m), ASTER GDEM, SRTM DEM, ALOS AW3D30 DEM, and two DEMs with low resolution (90 m), TanDEM-X and SRTM DEM, were used and the 2D root mean square error (RMSE) was calculated. The results showed that the most reliable DEM for landslide research is the DSM from the Greek Cadastral, while the least reliable ones were TanDEM-X and SRTM DEM, with a 90 m resolution.

Table 1 includes the DEM and DTM used in the landslide investigation, with the relevant spatial analysis, presented in chronological order.

According to the statistical analysis (Figure 4), in landslide assessments the most-used resolution is 10 m, with a percentage of approximately 22%, and the second is 30 m, with a rate of 20%. This is because, at local scales, a finer resolution is more appropriate and a 10 m pixel size is reasonably widely used. However, at regional scales, a smaller resolution is more appropriate and a 30 m pixel size is logical. DEMs with a spatial resolution of over 40 m were present at a rate of less than 2%, except for the 90 m resolution, which presented at a rate of 5%. The higher frequency of the use of the 90 m pixel size may be due to the SRTM DEM, which has 30 m and 90 m resolutions and is a well-known DEM with global uses. Rates from 7.5% to 10% were observed at 1 m, 5 m, 20 m, and 25 m, and frequently these are derived from resampling as researchers are aiming to create the best accuracy based on their demand. The rest of the cell sizes were remotely extracted at a rate less than 5%.

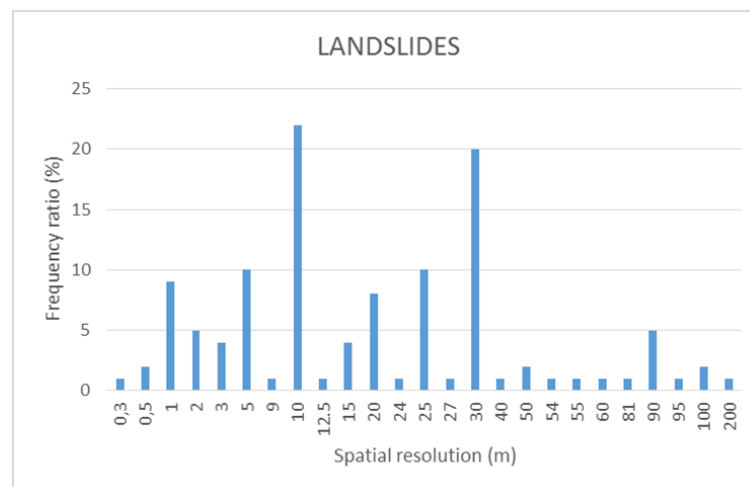


Figure 4. The frequency of spatial resolutions' use in landslide investigations.

Table 1. Resolutions used in landslide investigation.

Authors	Reference No.	Date	Resolution (m)	DEM Generation	DEM Name
Carrara et al.	[128]	1991	25	1:25,000 topographic map	DTM
Gao	[5]	1993	24	-	DEM
Borga et al.	[6]	1998	10	1:10,000 contour map	DEM
Pack et al.	[7]	1998	10	1:45,000 photographs	DEM
Guzzetti et al.	[88]	1999	25	1:25,000 topographic map	DTM
Agliardi et al.	[91]	2001	10	1:10,000 topographic map	DEM
Vanacker et al.	[49]	2003	5	1:10,000 topographic map	DEM
Jaboyedoff et al.	[9]	2004	25	1:25,000 national map	SWISSTOPO DEM
Gunther et al.	[76]	2004	5	-	ATKIS DGM5
Pesci et al.	[71]	2004	0.3	aerial photogrammetry	Photogrammetric DEM
			1	laser scanning data	DEM
			1	GPS data	DEM
Lee et al.	[108]	2004	5, 10, 30, 100, 200	-	DEM
Nichol et al.	[95]	2005	5	1:10,000 contour map	DEM
Yesilnacar et al.	[33]	2005	25	1:25,000 topographic maps	DEM
Lee et al.	[57]	2005	10	1:50,000 topographic map	DEM
Claessens et al.	[129]	2005	10, 25, 50, 100	-	DEM
Lee et al.	[63]	2006	10	topographic map	DEM
Ardizzone et al.	[72]	2007	2, 10	ALSM	LiDAR DEM
Gorsevski et al.	[32]	2008	30	-	DEM
Tarolli et al.	[100]	2009	1, 3, 5, 10, 20, 30	LiDAR data	LiDAR DTM
Jaboyedoff et al.	[42]	2009	0.5	air photo stereo pair at a scale of 1:12,000	DEM
Kawabata et al.	[19]	2009	15	ASTER satellite images	ASTER DEM
			55	Geographical Survey Institute (GSI) of Japan	DEM
Kasai et al.	[23]	2009	1	-	LiDAR-derived DEM

Table 1. Cont.

Authors	Reference No.	Date	Resolution (m)	DEM Generation	DEM Name
Pradhan et al.	[58]	2010	10	-	DEM
Miner et al.	[10]	2010	1, 2, 5	LiDAR datasets	LiDAR DEM
Mancini et al.	[85]	2010	40	aerial images	DEM
Martha et al.	[28]	2010	10	2.5 m Cartosat-1 imagery	DEM
Pradhan et al.	[56]	2010	10	1:25,000 topographic map	DEM
Mclean	[130]	2011	30	-	GTOPO DEM
			30	-	SRTM DEM
Keijesers et al.	[81]	2011	9, 27, 54, 81	-	DEM
Gorum et al.	[79]	2011	90	1:50,000 topographic map	DEM
Jaboyedoff et al.	[102]	2012	1	aerial laser scanning (ALS)	HRDEM
			2	aerial laser scanning (ALS)	HRDEM
			25	by a 1:25,000 national map	SWISSTOPO DEM
			15	resolution from resampling	LiDAR DEM
			10	resolution from degrading	HRDEM
Costanzo et al.	[29]	2012	10	-	DEM
Ozdemir et al.	[41]	2013	20	1:25,000 topographic map	DEM
Martha et al.	[38]	2013	10	Cartosat-1 data	DEM
Fenton et al.	[11]	2013	3	-	SRTM DEM
			30	-	GTOPO DEM
Oh et al.	[52]	2013	15	ASTER satellite images	ASTER DEM
Qin et al.	[111]	2013	25	1:10,000 topographic map	DEM
Chen et al.	[22]	2013	10, 20, 30, 60, 90	1:50,000 topographic map	DEM
Calvello et al.	[25]	2013	25	-	DEM
			95	-	SRTM DEM
Chandra et al.	[47]	2013	20	1:25,000 topographic map	DEM

Table 1. Cont.

Authors	Reference No.	Date	Resolution (m)	DEM Generation	DEM Name
Fuchs et al.	[46]	2014	10	TerraSAR-X data stereo pairs	GeoElevation10 DEM
			30	-	ASTER GDEM
Dagdelenler et al.	[34]	2015	25	1:25,000 topographic map	DEM
			10, 12.5	-	DEM
Ciampalini et al.	[48]	2015	20	Italian Military Geographic Institute (IGM)	IGM DEM
Mandal et al.	[27]	2015	25	1:50,000 topographic map	DEM
Huang et al.	[96]	2015	15	InSAR technique	DEM
			90	-	SRTM DEM
Chang K.T. et al.	[18]	2016	5	LiDAR data	LiDAR DEM
			30	-	ASTER DEM
Pawluszek et al.	[20]	2016	5	ISOK project	DEM
Mahalingam et al.	[21]	2016	10	LiDAR datasets	LiDAR DEM
Ciampalini et al.	[12]	2016	1, 2	ALS LiDAR data	ALS- LiDAR DEM
			20	Italian Military Geographic Institute (IGM)	IGM DEM
Mahalingam et al.	[60]	2016	1, 3, 5, 10, 30, 50	some resolutions are from resampling	ASTER, LiDAR and NED DEM
Rasyid et al.	[68]	2016	30	-	ASTER DEM
Wang et al.	[69]	2016	30	-	ASTER DEM
Pradhan et al.	[13]	2017	0.5, 1, 2, 3, 5, 10, 20, 30	LiDAR datasets	LiDAR DEM
			30	ASTER satellite images	ASTER DEM
Bianchini et al.	[87]	2017	20	TINITALY/01 DEM Project	TINITALY DEM
Liu et al.	[25]	2018	30	-	DEM
Zhu et al.	[39]	2018	30	1:50,000 topographic map	DEM
Juliev et al.	[70]	2019	30	-	ASTER DEM
Dou et al.	[40]	2019	10	-	DEM

Table 1. Cont.

Authors	Reference No.	Date	Resolution (m)	DEM Generation	DEM Name
Kakavas et al.	[80]	2020	5	Greek Cadastral	DSM from the Greek Cadastral
			30	-	ASTER GDEM
			30	-	ALOS AW3D30 DEM
			30	-	SRTM DEM
			90	-	SRTM DEM
			90	-	TanDEM-X

5.2. The Effect of DEM Resolution on Rockfalls

DEMs/DTMs with small, medium, or large pixel sizes have also been used for rockfall detection and validation in regional or large-scale occurrences. The resampling of resolution is also applied in rockfall studies [15,64,84,105,107,118]. A literature review according to the resolution of DEMs/DTMs in rockfalls is presented in the following paragraphs.

Acosta et al. (2002) created two rockfall maps, the first derived from morphometric assumptions and the second from aerial photo interpretation [89]. They achieved rockfall vulnerability mapping through a kinetic modeling approach in Aragona, Spain. STONE software offered a 3D simulation that was based on a lumped mass algorithm and edited as input data into a DEM with 25 m cell size.

Baillifard et al. (2003) analyzed five instability factors (fault, scree slope, rock cliff, steep slope, and road), aiming to produce a rockfall hazard map [44]. A DTM with 25 grid size was taken into account to extract the slope data. They concluded that a 25 m resolution does not provide detailed information on slope parameters and that a smaller grid size might be more appropriate.

Marquinez et al. (2003) assessed rockfall activity susceptibility in Northern Spain [131]. Rockfall conditioning factors, such as environmental and geological, and rockfall quantification factors, such as rockfall basin delimitation and rockfall activity indicators, were measured with the contribution of a 25 m resolution DEM created from a 1:25,000 topographic map. Finally, they mapped low- and high-activity zones in rock cliff units.

Agliardi et al. (2003) presented a 3D kinetic simulation approach through the STONE program with uploaded data from rockfalls in the Central Alps, Italy [105]. They input in the STONE software a 5 m DEM derived from a topographic map, 10 m and 20 m resolution DEMs that were resampled from the previous DEM, a 1 m DEM created from LiDAR techniques, and 5 m and 10 m resolution DEMs that were resampled from the LiDAR DEM. Multiresolution experiments provide basic information about accuracy at local or wider scales.

Guzzetti et al. (2003) surveyed rockfalls in Yosemite Valley, California, recording historical events over a period of 145 years, and computing rockfall hazards through the STONE program [106]. They achieved a 3D simulation approach by introducing, into STONE software, a 10 m DEM created from digitized contours on a 1:24,000-scale topographic map.

Crosta et al. (2003) applied a 3D modeling code from STONE software in regional and large-scale rockfalls in areas in Italy, aiming to achieve hazard assessment [107]. In the aforementioned program, DEMs are required as input data and the algorithm does not have spatial resolution limitations. Two DEMs were used, the first with 20 m resolution and the second with 5 m, which were resampled to 10 m and 20 m resolution. That resampling aimed to show how the resolution affected the hazard results; they concluded that the smaller cell size (5 m) gave an adequately detailed simulation of rockfall trajectories.

Guzzetti et al. (2004) accomplished rockfall risk assessment via the STONE program. They achieved the rockfall simulation by a lumped mass approach [66]. A DEM with 5 m pixel size, derived from a 1:10,000 scale topographic map, was input in the program. Finally, they concluded that in terrain that is very steep, DEMs created from topographic maps are not accurate, as the contour lines in these areas are not shown in topographic maps.

Crosta et al. (2004) evaluated rockfall trajectories via the use of STONE software, which accomplishes a 3D numerical modeling simulation [45]. Lateral dispersion, specifically macro- or microtopographic and dynamic factors and a kinematic module, were calculated and were illustrated with the use of four different DEMs with 1 m, 2 m, 3 m, and 4 m resolutions. They concluded that the DEMs' accuracy affects the lateral dispersion capture as the lateral dispersion from finer DEM increases with a slope of 45°.

Jaboyedoff et al. (2004) detected and qualified discontinuities in Switzerland [121]. They measured discontinuity sets of parameters through Matterocking software and illustrated possible rockslide zones. The topography of the area of interest was studied in two parts. The first was before the rockslide event and the second was after. These parts

were compared with the aid of a 25 m resolution DEM that exported topographic details and, consequently, discontinuity points. Finally, they determined that a DEM with higher resolution would detect more discontinuities.

Derron et al. (2005) described the required procedure for rockfall risk mapping using a DEM with 5 m resolution, generated by 1:15,000 scale aerial photographs [110]. Features such as erosion, structure, hydrology, the direction of discontinuities, mass movement, and block propagation were extracted by the aforementioned DEM and Colptop3D, Matterocking 2.0, and ConeFall software. The SLBL method was used for the measurement of the pressure exerted by the gravitational mass on the sloping local base plane.

Lan et al. (2006) simulated, in three dimensions, the kinetic process of a lumped mass, with the ultimate goal of mapping rockfall orbits [103]. A 1 m DEM derived from LiDAR data, aerial photographs, lumped mass, and Kriging methods extracted parameters such as surface morphology, topography, mass movements, velocities, etc. These procedures yielded a reliable rockfall risk assessment and a faithful 3D modeling approach.

Frattini et al. (2008) created a rockfall susceptibility map by using the 3D HY-STONE simulation code [82]. Aerial photographs were interpreted and a 10 m cell size DTM derived from contour lines was analyzed to develop an inventory map with stable, unstable, and unclassified areas. Geomorphological and empirical methods were integrated into the HY-STONE algorithm.

Loye et al. (2009) focused on the prediction of future rockfalls through the use of HRDEMs [15]. In situ observation and orthophotos analysis took place in the area of interest at Canton of Vaud, in Switzerland. The distribution of the slope angle that is derived from topographic and geological maps, in combination with GIS techniques and HRDEMs, has led to the desired goal. The cell size of the HRDEMs varied between 1 m to 25 m with a 5 m step, while the 25 m spatial resolution DEM constituted the typical Swiss DEM (Swisstopo). The researchers concluded that DEMs of higher resolution are more efficient for small-scale rockfalls, while for large-scale rockfalls, lower-resolution DEMs are more suitable.

Ravanel et al. (2010) gathered the characteristics of rockfalls at Mont Blanc Massif [84]. Some of the characteristics assessed were the site, date, location, elevation, slope, rocky type, aspect, deposit area, collapsed volume, maximum scar depth, permafrost occurrence, and ice seen in the scar. These were collected using aerial photographs at a scale of 1:20,000 and a 50 m DEM, which was resampled to 10 m resolution in the areas of occurrences to achieve higher accuracy.

Zieher et al. (2012) estimated three major rockfall parameters, disposal, orbit, and rubbing, for mass modeling and simulation [75]. They achieved their goal with the use of four DTMs (2.5 m, 5 m, 10 m, and 20 m) created from airborne laser scanning and found that a higher resolution is recommended for local-scale rockfalls, whereas lower is preferred for the regional scale due to the fact that the latter overestimates the slope angle values.

Palma et al. (2012) detected vulnerable areas in southern Italy and indicated rockfall hazard zones [99]. They achieved 2D and 3D rockfall simulation by taking advantage of the geomechanic characteristics of the area of interest. GeoRock 2D, Rotomap, and Stone 3D software were used for rockfall trajectory modeling. The 3D software exploited a DEM with 5 m resolution to accomplish the simulation.

Corona et al. (2013) achieved a 3D rockfall simulation by using RockyFor3D software [114]. In this program, a high-resolution DEM (2.5 m) derived from LiDAR data was input and potential rockfall areas were detected. The interaction of trees and rockfalls was discussed by studying an area in the Swiss Alps.

Frattini et al. (2013) took advantage of the HY-STONE code to achieve a 3D rockfall modeling calibration in Italian Alps [64]. They input, in this code, DEMs with different resolutions and observed the effect of the analysis on the results. More specifically, they used LiDAR DEM (1 m, 5 m, 10 m, and 20 m), TOPOGRID DEM (5 m, 10 m, and 20 m) and TIN-to-RASTER DEM (5 m, 10 m, and 20 m), which are derived from different algorithms

and consequently need individual cell size parameter sets. DEMs with lower accuracy led to longer runout simulation as opposed to higher ones.

Nikolakopoulos et al. (2015) assessed the rockfall risk by estimating the engineering geological conditions [104]. They accomplished a 2D rockfall simulation with RocFall software and a stereographic projection illustration with DIPS software. Factors such as kinetic energy, slope, etc. were extracted by an airphoto mosaic with 25 m resolution and a 5 m DEM. Their goal was to come up with appropriate preventive measures for these occasions.

Bühler et al. (2016) presented a 3D simulation of rockfall movement via the application of the RAMMS and GIS software [118]. DEMs with 0.25 m, 0.5 m, 1 m, 2 m, 5 m, and 10 m cell size were uploaded in RAMMS for the extraction of rock action. They noticed that the cell size does not affect the simulation outcomes in flatter areas. Contrary to the above, the cell size affects the results in areas of roughness and, for that reason, the use of finer resolution is recommended on this occasion.

Žabota et al. (2019) examined the impact of DEMs' resolution on the detection and validation of rockfalls' creation, transportation, and deposition [101]. The software Conefall and five DEMs (1 m, 5 m, 12.5 m, 25 m, and 100 m) were taken into account in this procedure, while the area of interest, in Slovenia, was divided into two zones based on its lithology. The conclusions were that DEMs of 1 m and 5 m resolution are suitable for small-scale rockfall events, DEMs with 12.5 and 25 m are appropriate for large scales, and finally the DEM with 100 m is inappropriate for this type of study due to its very low accuracy.

Table 2 includes the DEM and DTM used for the rockfall investigation, with the relevant spatial analysis, in chronological order.

According to the statistical analysis (Figure 5), in rockfall assessments the most often used resolutions are 5 m and 10 m, at rates of 15% and 12%, respectively, and 20 m, with a rate of 8%. DEMs with 1 m and 25 m resolutions presented at rates of 7% and 6%, respectively, while the rest of the resolutions had a rate less than 2%. In rockfall investigations, we noticed the same trend as with landslides. In local-scale events, the use of a finer resolution was observed, which accounted for the 12% or higher rates at 5 m and 10 m. By contrast, at regional scales, a coarser resolution is preferred; this explains the frequent use of 20 m and 25 m resolutions.

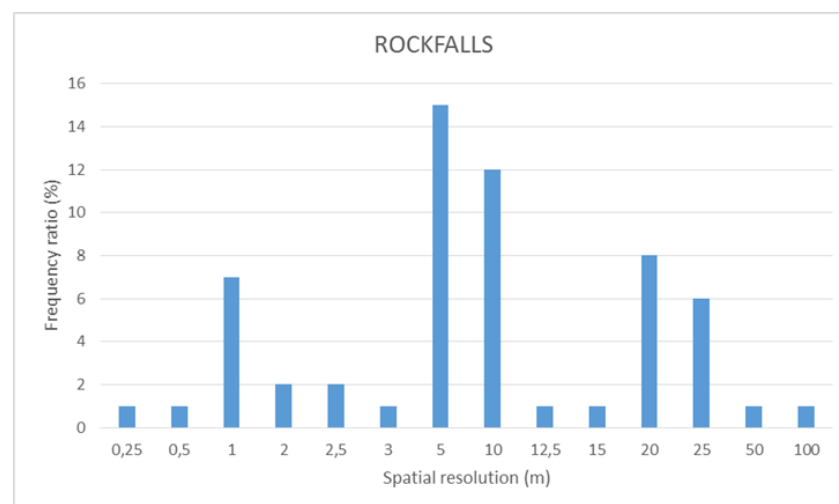


Figure 5. The frequency of use of different spatial resolutions in rockfall investigations.

Table 2. Resolutions used for rockfall investigation.

Authors	Reference No.	Date	Resolution (m)	DEM Generation	DEM Name
Baillifard et al.	[89]	1999	25	1:25,000 Swiss topographic maps	DTM
Acosta et al.	[44]	2002	25	-	DEM
Marquinez et al.	[131]	2003	25	1:25,000 topographic map	DEM
Agliardi et al.	[105]	2003	5	1:5000 topographic map	TOPO DEM
			10, 20	resolution from resampling	DEM
			1	aerial laser scanning (ALS)	LiDAR DEM
			5, 10	resolution from resampling	DEM
Guzzetti et al.	[106]	2003	10	1:24,000 topographic contour lines	USGS DEM
			20	1:10,000 topographic map	DEM
Crosta et al.	[107]	2003	5	1:5000 topographic map	DEM
			10, 20	resolution from resampling	DEM
Guzzetti et al.	[66]	2004	5	1:10,000 topographic map	DEM
Crosta et al.	[45]	2004	1, 2, 3, 5	-	DEM
Jaboyedoff et al.	[121]	2004	25	-	DEM
Derron et al.	[110]	2005	5	1:15,000 scale aerial photographs	DEM
Lan et al.	[103]	2006	1	LiDAR data	LiDAR DEM
Frattini et al.	[82]	2008	10	contour lines	DTM
Loye et al.	[15]	2009	1, 5, 10, 15, 20, 25	-	HRDEMs
Ravanel et al.	[84]	2010	50	-	DEM
			10	resolution from resampling	DEM
Zieher et al.	[75]	2012	2.5, 5, 10, 20	by ALS	ALS DTM
Palma et al.	[99]	2012	5	-	DEM
Corona et al.	[114]	2013	2.5	LiDAR data	LiDAR DEM
Frattini et al.	[64]	2013	1, 5, 10, 20	-	LiDAR DEM
			5, 10, 20	-	TOPOGRID DEM
			5, 10, 20	-	TIN-to-RASTER DEM
Nikolakopoulos et al.	[104]	2015	5	-	DEM
Bühler et al.	[118]	2016	0.25, 0.5, 1, 2, 5, 10	-	DEM
Žabota et al.	[101]	2019	1	laser surface imaging	LiDAR DEM
			5, 12.5, 25, 100	-	official DEMs of Slovenia

6. Conclusions

In order to investigate landslide/rockfall phenomena, certain steps must be followed. Factors, models, software, and DEMs hold the key to successful vulnerability mapping and all of them are connected, either directly or indirectly. Over the years, the advancements of methods, software, and resolution mentioned above have given researchers the opportunity to choose the most suitable ones, based on the demands of the area and the goal. This study focused on the collection of scientific articles pertaining to DEMs' resolution in landslide/rockfall surveys. This material was obtained mainly from the Google Scholar, Research Gate, and Scopus platforms, for composing a literature review of those most popular and most relevant to rockslide studies. Finally, a statistical analysis was accomplished via Excel software.

Causative, predictive, and topographic factors are points of reference regarding landslide studies as the stability of an area can be tested by these indexes. The effects of these factors vary and can affect the accuracy of the analysis [58]. According to this work, the most calculated topographic index, included in one-third of the investigations analyzed, is the slope, whose measurement is affected by DEMs' resolution [17]. In addition, the veg-

etation index, NDVI, has been taken into account by many researchers as it affects the hazard risk zone. Furthermore, the topographic indexes TPI, TWI, TRI, CTI, STI, and SPI all play a significant role in landslide mapping [17], and their presence in a survey depends on the scope of each researcher. Given the above, the most commonly used index is TWI, which appeared at a rate of 17%.

Landslide susceptibility mapping can be achieved through the use of models and, thus, a large variety of different models have been developed. The most common method, based on a statistical analysis of the read papers, is API. The interferometry of aerial photos (API) is the key to present and future studies. Eighteen percent of the works included chose this method as the extraction of the previous condition of a vulnerable area can be obtained easily. The second most common is the satellite imagery (SI) method, with a rate of 12%. Landslide inventory maps can be created with the use of satellite images [95]. The DEM input affects the results of any method, and this restriction has been taken into consideration by researchers.

Nowadays, rockslide software is a useful tool due to the availability of multiple parameters of input data, as DEMs' or DTMs' resolution can be resampled, either in coarser or in finer resolution, to satisfy all the landslides' or rockfalls' requirements. A resampling can achieve a higher resolution and, consequently, a smaller cell size can better illustrate a detailed simulation of rockfall trajectories [107]. The most used software, with a rate of one-quarter of the surveys analyzed, is STONE, which simulates rockfall trajectories and has the advantage that its algorithm does not have spatial resolution limitations [107]. CONEFALL software was used by 16% as it is a more suitable software for regional-scale rockfall propagation. Additionally, it is compatible with the GIS environment and produces credible results in a short time [126].

The necessity of DEMs in landslide/rockfall investigations, for prediction at either small or large scales, was underlined by many researchers [67,78,132]. Having accomplished this literature review, the necessity of DEMs in this type of research is undeniable, but some limitations should be taken into account. For example, in terrains that are very steep, the DEMs that can be created from topographic maps are not accurate, as contour lines in these areas are not shown on topographic maps [66]. Hence, DEMs with low accuracy flatten the topography's roughness and, consequently, decrease the reliability of the prediction area [81]. In addition, DEMs with higher accuracy export more detailed outcomes for the majority of landslide factors, but this is not the case for every analysis [13].

Having studied more than 200 papers that analyze landslides and rockfalls (in terrestrial environments) with the use of DEMs/DTMs, the conclusion is that the spatial resolution affects the reliability of the results and depends on the scale. There is no "bad" or "good" resolution but just "appropriate" or "not appropriate" according to the landslide/rockfall goal that each researcher wants to achieve and to the pre-existing offered data. If the survey is of local-scale events, DEMs with a resolution of 5 m or 10 m are preferred at a rate of over 20%, while for regional-scale DEMs resolutions of 20 m or 30 m are preferred at a rate of less than 20%. This conclusion was also confirmed by a previous study that concluded that the most used DEMs according to their literature review had a spatial resolution of less than 25 m and that DEMs with 30 m resolution are appropriate for large-scale events and DEMs with 5 m are for coarse scale as they better capture the morphometric details [53]. Finally, DEMs with resolutions larger than 100 m are neither appropriate for rockfall nor for landslide detection; this explains the low rate of less than 2%.

The most acceptable grid size is around 10 m spatial resolution as it offers a detailed cartography of landslides/rockfalls. DEMs with very high resolution are quite expensive and thus it is difficult to cover large areas. DEMs with grid sizes such as 0.5 m, 1 m, 2 m, and 5 m are only suitable for large-scale mapping of very small areas. For larger areas, DEMs with coarse resolutions (e.g., 90 m or 100 m) are more often used; however, they do not provide an accurate representation of the relief. A DEM with 10 m spatial resolution is appropriate for any landslide/rockfall scale. Moreover, the grid size of DEMs does not

affect the time of simulation on rockfall software, so the resolution does not constitute a restriction for the choice of the input DEM.

7. Future Work

Rockslides are not only terrestrial but also extraterrestrial geomorphological phenomena. Various space agencies (NASA, ESA, ISRO, etc.) and private firms (SpaceX, Virgin Galactic, Blue Origin, etc.) have set the stage for a new space era that will involve the mining of other planetary bodies (among other goals) like Mars and the Moon. To this end, the prone-to-landslide areas upon the Martian and lunar surfaces must be clearly determined, since it would be quite risky for a prospective space mission to set up on such harsh and unstable areas. A HRSC DEM (with a grid cell of 50–150 m) and a MOLA DEM (with a grid cell of 463 m) have been used, aiming to extract morphometric parameters regarding Martian landslides, and a database of 3118 Martian landslides has been created [133]. It is concluded that slope angles are underestimated when a low-resolution DEM is applied. The physical and mechanical characteristics of the Martian and lunar soil (regolith) [134,135], are parameters closely connected with landslide mechanisms that affect their initiation. Hence, the more information that is gathered, the more data will be available for future extraterrestrial landslide investigations. As scientists focus on other planetary bodies through the years, an increasing number of DEMs will be developed for the susceptibility mapping of such hazardous (in terms of landslides) extraterrestrial surfaces, and that will be the beginning of a new era for interplanetary remote sensing.

Author Contributions: Conceptualization, M.P.K. and K.G.N.; methodology, M.P.K.; formal analysis, M.P.K.; resources, M.P.K. and K.G.N.; writing—original draft preparation, M.P.K.; writing—review and editing, K.G.N.; visualization, M.P.K.; supervision, K.G.N.; project administration, K.G.N.; funding acquisition, K.G.N. All authors have read and agreed to the published version of the manuscript.

Funding: This research was supported by a grant (no. 80634) from the Research Committee of the University of Patras via the “C. Caratheodori” program.

Institutional Review Board Statement: Not applicable.

Informed Consent Statement: Not applicable.

Data Availability Statement: Not applicable.

Acknowledgments: We would like to thank the Research Committee of the University of Patras for funding via the “C. Caratheodori” program.

Conflicts of Interest: The authors declare no conflict of interest.

Abbreviations

Acronyms	Meaning
MODELS	
DEM	Digital Elevation Model
DTM	Digital Terrain Model
DSM	Digital Surface Model
INDEXES	
TPI	Topographic Position Index
TWI	Topographic Wetness Index
TRI	Topographic Roughness Index
CTI	Compound Topographic Index
STI	Sediment Transport Index
SPI	Stream Power Index
NDVI	Normalized Difference Vegetation Index
SL	Slope

METHODS

AHP	Analytical Hierarchy Process
PLR	Probabilistic Likelihood Ratio
FM	Fuzzy Method
HL	Hybrid Likelihood
TIN	Triangular Irregular Networks
ANN	Artificial Neural Networks
FBPNN	Feedforward Back-Propagation Neural Network
AUC	Area under the Curve
ROC	Receiver Operating Characteristic
GPS	Ground Position System
API	Aerial Photo Interpretation
TPI	Terrestrial Photo Interpretation
InSAR	Satellite Radar Interferometry
SI	Satellite Imagery
ALS	Aerial Laser Scanning
TLS	Terrestrial Laser Scanning
LiDAR	Light Detection and Ranging
KM	Kriging Method
LM	Lumped Mass Method
WofE	Weights of Evidence
FR	Frequency Ratio
CF	Certainty Factor
DA	Discriminant Analysis
LR	Logical Regression
MM	Matrix Method
RFEM	Random Finite Element Method
SLBL	Sloping Local Base Level
MCM	Monte Carlo Method
DEM/DTM	
ALOS	Advanced Land Observing Satellite
SRTM	Shuttle Radar Topography Mission
ASTER	Advanced Spaceborne Thermal Emission and Reflection Radiometer
TanDEM-X	TerraSAR-X add-on for Digital Elevation Measurement
MOLA	Mars Orbiter Laser Altimeter
HRSC	High-Resolution Stereo Camera on Mars Express

References

1. Florinsky, I.V. Accuracy of local topographic variables derived from digital elevation models. *Int. J. Geogr. Inf. Sci.* **1998**, *12*, 47–62. [[CrossRef](#)]
2. Maune, D.F.; Maitra, J.B.; McKay, E.J. Accuracy Standards. In *Digital Elevation Models and Applications: The DEM Users Manual*; American Society for Photogrammetry and Remote Sensing: Bethesda, MD, USA, 2001; pp. 61–82.
3. Sauchyn, D.J.; Gardner, J.S. Morphometry of open rock basins, Kananaskis area, Canadian Rocky Mountains. *Can. J. Earth Sci.* **1983**, *20*, 409–419. [[CrossRef](#)]
4. Toppe, R. Terrain models: A tool for natural hazard mapping. *IAHS Publication* **1987**, *162*, 629–638.
5. Gao, J. Identification of topographic settings conducive to landsliding from dem in Nelson county, Virginia, USA. *Earth Surf. Process. Landf.* **1993**, *18*, 579–591. [[CrossRef](#)]
6. Borga, M.; Dalla Fontana, G.; Da Ros, D.; Marchi, L. Shallow landslide hazard assessment using a physically based model and digital elevation data. *Environ. Geol.* **1998**, *35*, 81–88. [[CrossRef](#)]
7. Pack, R.T.; Tarboton, D.G.; Goodwin, C.N. The SINMAP Approach to Terrain Stability Mapping. In Proceedings of the 8th Congress of the International Association of Engineering Geology, Vancouver, BC, Canada, 21–25 September 1998.
8. Dietrich, W.E.; Bellugi, D.G.; Sklar, L.S.; Stock, J.D.; Heimsath, A.M.; Roering, J.J. Geomorphic Transport Laws for Predicting Landscape form and Dynamics. *Geophys. Monogr. Ser.* **2013**, 103–132. [[CrossRef](#)]
9. Jaboyedoff, M.; Baillifard, F.; Couture, R.; Locat, J.; Locat, P. Toward preliminary hazard assessment using DEM topographic analysis and simple mechanical modeling by means of sloping local base level. Part B. In *Landslides Evaluation and Stabilization*; Balkema: Boca Raton, FL, USA, 2004; pp. 199–205.
10. Miner, A.; Flentje, P.; Mazengarb, C.; Windle, D.J. Landslide Recognition Using LiDAR Derived Digital Elevation Models-Lessons Learnt from Selected Australian Examples. In Proceedings of the 11th IAEG Congress of the International Association of Engineering Geology and the Environment, Auckland, New Zealand, 5–10 September 2010; pp. 1–9.

11. Fenton, G.A.; McLean, A.; Nadim, F.; Griffiths, D.V. Landslide hazard assessment using digital elevation models. *Can. Geotech. J.* **2013**, *50*, 620–631. [[CrossRef](#)]
12. Ciampalini, A.; Raspini, F.; Frodella, W.; Bardi, F.; Bianchini, S.; Moretti, S. The effectiveness of high-resolution LiDAR data combined with PSInSAR data in landslide study. *Landslides* **2015**, *13*, 399–410. [[CrossRef](#)]
13. Pradhan, B.; Sameen, M.I. Effects of the Spatial Resolution of Digital Elevation Models and Their Products on Landslide Susceptibility Mapping. *Laser Scanning Appl. Landslide Assess.* **2017**, 133–150. [[CrossRef](#)]
14. Depountis, N.; Nikolakopoulos, K.; Kavoura, K.; Sabatakakis, N. Description of a GIS-based rockfall hazard assessment methodology and its application in mountainous sites. *Bull. Eng. Geol. Environ.* **2019**. [[CrossRef](#)]
15. Loye, A.; Jaboyedoff, M.; Pedrazzini, A. Identification of potential rockfall source areas at a regional scale using a DEM-based geomorphometric analysis. *Nat. Hazards Earth Syst. Sci.* **2009**, *9*, 1643–1653. [[CrossRef](#)]
16. Jaboyedoff, M.; Baillifard, F.; Couture, R.; Locat, J.; Locat, P. Toward preliminary hazard assessment using DEM topographic analysis and simple mechanical modeling by means of sloping local base level. Part A. In *Landslides Evaluation and Stabilization*; Balkema: Boca Raton, FL, USA, 2004; pp. 191–198.
17. Saleem, N.; Huq, M.; Twumasi, N.Y.D.; Javed, A.; Sajjad, A. Parameters derived from and/or used with digital elevation models (DEMs) for landslide susceptibility mapping and landslide risk assessment: A review. *ISPRS Int. J. Geo Inf.* **2019**, *8*, 545. [[CrossRef](#)]
18. Chang, K.T.; Doub, J.; Chang, Y.; Kuo, C.P.; Xu, K.M.; Liu, J.K. Spatial resolution effects of digital terrain models on landslide susceptibility analysis. *Int. Arch. Photogramm. Remote Sens. Spat. Inf. Sci.* **2016**, *8*. [[CrossRef](#)]
19. Kawabata, D.; Bandibas, J. Landslide susceptibility mapping using geological data, a DEM from ASTER images and an Artificial Neural Network (ANN). *Geomorphology* **2009**, *113*, 97–109. [[CrossRef](#)]
20. Pawluszek, K.; Borkowski, A. Impact of DEM-derived factors and analytical hierarchy process on landslide susceptibility mapping in the region of Rożnów Lake, Poland. *Nat. Hazards* **2017**, *86*, 919–952. [[CrossRef](#)]
21. Mahalingam, R.; Olsen, M.J.; O'Banion, M.S. Evaluation of landslide susceptibility mapping techniques using lidar-derived conditioning factors (Oregon case study). *Geomat. Nat. Hazards Risk* **2016**, *7*, 1884–1907. [[CrossRef](#)]
22. Chen, Q.; Liu, X.; Liu, C.; Ji, R. Impact Analysis of Different Spatial Resolution DEM on Object-Oriented Landslide Extraction from High Resolution Remote Sensing Images. In Proceedings of the 2013 Ninth International Conference on Natural Computation (ICNC), Shenyang, China, 23–25 July 2013; IEEE: pp. 940–945. [[CrossRef](#)]
23. Kasai, M.; Ikeda, M.; Asahina, T.; Fujisawa, K. LiDAR-derived DEM evaluation of deep-seated landslides in a steep and rocky region of Japan. *Geomorphology* **2009**, *113*, 57–69. [[CrossRef](#)]
24. Ku, C.Y. Assessing Rockfall Hazards Using a Three-Dimensional Numerical Model Based on High Resolution DEM. In Proceedings of the Twenty-second International Offshore and Polar Engineering Conference, Rhodes, Greece, 17–22 June 2012; International Society of Offshore and Polar Engineers: Cupertino, CA, USA.
25. Calvello, M.; Cascini, L.; Mastroianni, S. Landslide zoning over large areas from a sample inventory by means of scale-dependent terrain units. *Geomorphology* **2013**, *182*, 33–48. [[CrossRef](#)]
26. Corominas, J.; van Westen, C.; Frattini, P.; Cascini, L.; Malet, J.-P.; Fotopoulou, S.; Catani, F.; Van Den Eeckhaut, M.; Mavrouli, O.; Smith, J.T. Recommendations for the quantitative analysis of landslide risk. *Bull. Eng. Geol. Environ.* **2013**. [[CrossRef](#)]
27. Mandal, S.; Maiti, R. *Semi-Quantitative Approaches for Landslide Assessment and Prediction*; Springer: Singapore, 2015; pp. 57–93. [[CrossRef](#)]
28. Martha, T.R.; Kerle, N.; Jetten, V.; van Westen, C.J.; Kumar, K.V. Characterising spectral, spatial and morphometric properties of landslides for semi-automatic detection using object-oriented methods. *Geomorphology* **2010**, *116*, 24–36. [[CrossRef](#)]
29. Costanzo, D.; Rotigliano, E.; Irigaray, C.; Jiménez-Perálvarez, J.D.; Chacón, J. Factors selection in landslide susceptibility modelling on large scale following the gis matrix method: Application to the river Beiro basin (Spain). *Nat. Hazards Earth Syst. Sci.* **2012**, *12*, 327–340. [[CrossRef](#)]
30. Oh, H.J.; Kadavi, P.R.; Lee, C.W.; Lee, S. Evaluation of landslide susceptibility mapping by evidential belief function, logistic regression and support vector machine models. *Geomat. Nat. Hazards Risk* **2018**, *9*, 1053–1070. [[CrossRef](#)]
31. Ercanoglu, M.; Gokceoglu, C. Use of fuzzy relations to produce landslide susceptibility map of a landslide prone area (West Black Sea Region, Turkey). *Eng. Geol.* **2004**, *75*, 229–250. [[CrossRef](#)]
32. Gorsevski, P.V.; Jankowski, P. Discerning landslide susceptibility using rough sets. *Comput. Environ. Urban Syst.* **2008**, *32*, 53–65. [[CrossRef](#)]
33. Yesilnacar, E.; Topal, T. Landslide susceptibility mapping: A comparison of logistic regression and neural networks methods in a medium scale study, Hendek region (Turkey). *Eng. Geol.* **2005**, *79*, 251–266. [[CrossRef](#)]
34. Dagdelenler, G.; Nefeslioglu, H.A.; Gokceoglu, C. Modification of seed cell sampling strategy for landslide susceptibility mapping: An application from the Eastern part of the Gallipoli Peninsula (Canakkale, Turkey). *Bull. Eng. Geol. Environ.* **2015**, *75*, 575–590. [[CrossRef](#)]
35. Liu, J.; Duan, Z. Quantitative Assessment of Landslide Susceptibility Comparing Statistical Index, Index of Entropy, and Weights of Evidence in the Shangnan Area, China. *Entropy* **2018**, *20*, 868. [[CrossRef](#)]
36. Chen, W.; Panahi, M.; Tsangaratos, P.; Shahabi, H.; Ilia, I.; Panahi, S.; Li, S.; Jaafari, A.; Ahmad, B.B. Applying population-based evolutionary algorithms and a neuro-fuzzy system for modeling landslide susceptibility. *CATENA* **2019**, *172*, 212–231. [[CrossRef](#)]
37. Pourghasemi, H.R.; Mohammady, M.; Pradhan, B. Landslide susceptibility mapping using index of entropy and conditional probability models in GIS: Safarood Basin, Iran. *CATENA* **2012**, *97*, 71–84. [[CrossRef](#)]

38. Martha, T.R.; van Westen, C.J.; Kerle, N.; Jetten, V.; Vinod Kumar, K. Landslide hazard and risk assessment using semi-automatically created landslide inventories. *Geomorphology* **2013**, *184*, 139–150. [[CrossRef](#)]
39. Zhu, A.-X.; Miao, Y.; Yang, L.; Bai, S.; Liu, J.; Hong, H. Comparison of the presence-only method and presence-absence method in landslide susceptibility mapping. *CATENA* **2018**, *171*, 222–233. [[CrossRef](#)]
40. Dou, J.; Yunus, A.P.; Tien Bui, D.; Merghadi, A.; Sahana, M.; Zhu, Z.; Chen, C.-W.; Khosravi, K.; Yang, Y.; Pham, B.T. Assessment of advanced random forest and decision tree algorithms for modeling rainfall-induced landslide susceptibility in the Izu-Oshima Volcanic Island, Japan. *Sci. Total Environ.* **2019**. [[CrossRef](#)]
41. Ozdemir, A.; Altural, T. A comparative study of frequency ratio, weights of evidence and logistic regression methods for landslide susceptibility mapping: Sultan Mountains, SW Turkey. *J. Asian Earth Sci.* **2013**, *64*, 180–197. [[CrossRef](#)]
42. Jaboyedoff, M.; Couture, R.; Locat, P. Structural analysis of Turtle Mountain (Alberta) using digital elevation model: Toward a progressive failure. *Geomorphology* **2009**, *103*, 5–16. [[CrossRef](#)]
43. Van Dijke, J.J.; van Westen, C.J. Rockfall hazard: A geomorphologic application of neighbourhood analysis with ILWIS. *ITC J.* **1990**, *1*, 40–44.
44. Baillifard, F.; Jaboyedoff, M.; Sartori, M. Rockfall hazard mapping along a mountainous road in Switzerland using a GIS-based parameter rating approach. *Nat. Hazards Earth Syst. Sci.* **2003**, *3*, 435–442. [[CrossRef](#)]
45. Crosta, G.B.; Agliardi, F. Parametric evaluation of 3D dispersion of rockfall trajectories. *Nat. Hazards Earth Syst. Sci.* **2004**, *4*, 583–598. [[CrossRef](#)]
46. Fuchs, M.; Torizin, J.; Kühn, F. The effect of DEM resolution on the computation of the factor of safety using an infinite slope model. *Geomorphology* **2014**, *224*, 16–26. [[CrossRef](#)]
47. Devkota, K.C.; Regmi, A.D.; Pourghasemi, H.R.; Yoshida, K.; Pradhan, B.; Ryu, I.C.; Dhital, M.R.; Althuwaynee, O.F. Landslide susceptibility mapping using certainty factor, index of entropy and logistic regression models in GIS and their comparison at Mugling–Narayanghat road section in Nepal Himalaya. *Nat. Hazards* **2012**, *65*, 135–165. [[CrossRef](#)]
48. Ciampalini, A.; Raspini, F.; Bianchini, S.; Frodella, W.; Bardi, F.; Lagomarsino, D.; Di Traglia, F.; Moretti, S.; Proietti, C.; Pagliara, P. Remote sensing as tool for development of landslide databases: The case of the Messina Province (Italy) geodatabase. *Geomorphology* **2015**, *249*, 103–118. [[CrossRef](#)]
49. Vanacker, V.; Vanderschaeghe, M.; Govers, G.; Willems, E.; Poesen, J.; Deckers, J.; De Bievre, B. Linking hydrological, infinite slope stability and land-use change models through GIS for assessing the impact of deforestation on slope stability in high Andean watersheds. *Geomorphology* **2003**, *52*, 299–315. [[CrossRef](#)]
50. Yilmaz, I. Landslide susceptibility mapping using frequency ratio, logistic regression, artificial neural networks and their comparison: A case study from Kat landslides (Tokat—Turkey). *Comput. Geosci.* **2009**, *35*, 1125–1138. [[CrossRef](#)]
51. Chacón, J.; Irigaray, C.; Fernández, T.; El Hamdouni, R. Engineering geology maps: Landslides and geographical information systems. *Bull. Eng. Geol. Environ.* **2006**, *65*, 341–411. [[CrossRef](#)]
52. Oh, H.-J.; Park, N.-W.; Lee, S.-S.; Lee, S. Extraction of landslide-related factors from ASTER imagery and its application to landslide susceptibility mapping. *Int. J. Remote Sens.* **2012**, *33*, 3211–3231. [[CrossRef](#)]
53. Reichenbach, P.; Rossi, M.; Malamud, B.D.; Mihir, M.; Guzzetti, F. A review of statistically-based landslide susceptibility models. *Earth Sci. Rev.* **2018**, *180*, 60–91. [[CrossRef](#)]
54. Kaur, H.; Gupta, S.; Parkash, S.; Thapa, R. Application of geospatial technologies for multi-hazard mapping and characterization of associated risk at local scale. *Ann. GIS* **2018**, *24*, 33–46. [[CrossRef](#)]
55. Cascini, L.C.J.R.J.O.; Bonnard, C.; Corominas, J.; Jibson, R.; Montero-Olarte, J. Landslide hazard and risk zoning for urban planning and development. In *Landslide Risk Management*; Taylor and Francis: London, UK, 2005; pp. 199–235.
56. Pradhan, B.; Sezer, E.A.; Gokceoglu, C.; Buchroithner, M.F. Landslide Susceptibility Mapping by Neuro-Fuzzy Approach in a Landslide-Prone Area (Cameron Highlands, Malaysia). *IEEE Trans. Geosci. Remote Sens.* **2010**, *48*, 4164–4177. [[CrossRef](#)]
57. Lee, S.; Talib, J.A. Probabilistic landslide susceptibility and factor effect analysis. *Environ. Geol.* **2005**, *47*, 982–990. [[CrossRef](#)]
58. Pradhan, B.; Lee, S. Landslide susceptibility assessment and factor effect analysis: Backpropagation artificial neural networks and their comparison with frequency ratio and bivariate logistic regression modelling. *Environ. Model. Softw.* **2010**, *25*, 747–759. [[CrossRef](#)]
59. Niethammer, U.; James, M.R.; Rothmund, S.; Travelletti, J.; Joswig, M. UAV-based remote sensing of the Super-Sauze landslide: Evaluation and results. *Eng. Geol.* **2012**, *128*, 2–11. [[CrossRef](#)]
60. Mahalingam, R.; Olsen, M.J. Evaluation of the influence of source and spatial resolution of DEMs on derivative products used in landslide mapping. *Geomat. Nat. Hazards Risk* **2015**, *7*, 1835–1855. [[CrossRef](#)]
61. Akgun, A.; Dag, S.; Bulut, F. Landslide susceptibility mapping for a landslide-prone area (Findikli, NE of Turkey) by likelihood-frequency ratio and weighted linear combination models. *Environ. Geol.* **2007**, *54*, 1127–1143. [[CrossRef](#)]
62. Bagherzadeh, A.; Mansouri Daneshvar, M.R. Mapping of landslide hazard zonation using GIS at Golestan watershed, northeast of Iran. *Arab. J. Geosci.* **2012**, *6*, 3377–3388. [[CrossRef](#)]
63. Lee, S.; Ryu, J.-H.; Lee, M.-J.; Won, J.-S. The Application of Artificial Neural Networks to Landslide Susceptibility Mapping at Janghung, Korea. *Math. Geol.* **2006**, *38*, 199–220. [[CrossRef](#)]
64. Frattini, P.; Crosta, G.B.; Agliardi, F.; Imposimato, S. Challenging Calibration in 3D Rockfall Modelling. *Landslide Sci. Pract.* **2013**, 169–175. [[CrossRef](#)]

65. Stock, G.M.; Bawden, G.W.; Green, J.K.; Hanson, E.; Downing, G.; Collins, B.D.; Bond, S.; Leslar, M. High-resolution three-dimensional imaging and analysis of rock falls in Yosemite Valley, California. *Geosphere* **2011**, *7*, 573–581. [[CrossRef](#)]
66. Guzzetti, F.; Reichenbach, P.; Ghigi, S. Rockfall Hazard and Risk Assessment: Along a Transportation Corridor in the Nera Valley, Central Italy. *Environ. Manag.* **2004**, *34*, 191–208. [[CrossRef](#)]
67. Van Westen, C.J.; van Asch, T.W.J.; Soeters, R. Landslide hazard and risk zonation—why is it still so difficult? *Bull. Eng. Geol. Environ.* **2005**, *65*, 167–184. [[CrossRef](#)]
68. Rasyid, A.R.; Bhandary, N.P.; Yatabe, R. Performance of frequency ratio and logistic regression model in creating GIS based landslides susceptibility map at Lompobattang Mountain, Indonesia. *Geoenviro. Dis.* **2016**, *3*. [[CrossRef](#)]
69. Wang, Q.; Li, W.; Wu, Y.; Pei, Y.; Xie, P. Application of statistical index and index of entropy methods to landslide susceptibility assessment in Gongliu (Xinjiang, China). *Environ. Earth Sci.* **2016**, *75*. [[CrossRef](#)]
70. Juliev, M.; Mergili, M.; Mondal, I.; Nurtaev, B.; Pulatov, A.; Hübl, J. Comparative analysis of statistical methods for landslide susceptibility mapping in the Bostanlik District, Uzbekistan. *Sci. Total Environ.* **2018**. [[CrossRef](#)]
71. Pesci, A.; Baldi, P.; Bedin, A.; Casula, G.; Cenni, N.; Fabris, M.; Loddo, F.; Moram, M.; Bacchetti, M. Digital elevation models for landslide evolution monitoring: Application on two areas located in the Reno River Valley (Italy). *Ann. Geophys.* **2004**, *74*, 4. Available online: <http://hdl.handle.net/2122/836> (accessed on 8 April 2021).
72. Ardizzone, F.; Cardinali, M.; Galli, M.; Guzzetti, F.; Reichenbach, P. Identification and mapping of recent rainfall-induced landslides using elevation data collected by airborne Lidar. *Nat. Hazards Earth Syst. Sci.* **2007**, *7*, 637–650. [[CrossRef](#)]
73. Jaboyedoff, M.; Oppikofer, T.; Abellán, A.; Derron, M.-H.; Loye, A.; Metzger, R.; Pedrazzini, A. Use of LIDAR in landslide investigations: A review. *Nat. Hazards* **2010**, *61*, 5–28. [[CrossRef](#)]
74. Colesanti, C.; Wasowski, J. Investigating landslides with space-borne Synthetic Aperture Radar (SAR) interferometry. *Eng. Geol.* **2006**, *88*, 173–199. [[CrossRef](#)]
75. Zieher, T.; Formanek, T.; Bremer, M.; Meissl, G.; Rutzinger, M. Digital Terrain Model Resolution and its Influence on Estimating the Extent of Rockfall Areas. *Trans. GIS* **2012**, *16*, 691–699. [[CrossRef](#)]
76. Günther, A.; Carstensen, A.; Pohl, W. Automated sliding susceptibility mapping of rock slopes. *Nat. Hazards Earth Syst. Sci.* **2004**, *4*, 95–102. [[CrossRef](#)]
77. Read, R.S.; Langenberg, W.; Cruden, D.; Field, M.; Stewart, R.; Bland, H.; Chen, Z.; Froese, C.R.; Cavers, D.S.; Bidwell, A.K. Frank Slide a century later: The Turtle Mountain monitoring project. In *Landslide Risk Management*; CRC Press: Boca Raton, FL, USA, 2005; pp. 713–723.
78. Glenn, N.F.; Streutker, D.R.; Chadwick, D.J.; Thackray, G.D.; Dorsch, S.J. Analysis of LiDAR-derived topographic information for characterizing and differentiating landslide morphology and activity. *Geomorphology* **2006**, *73*, 131–148. [[CrossRef](#)]
79. Gorum, T.; Fan, X.; van Westen, C.J.; Huang, R.Q.; Xu, Q.; Tang, C.; Wang, G. Distribution pattern of earthquake-induced landslides triggered by the 12 May 2008 Wenchuan earthquake. *Geomorphology* **2011**, *133*, 152–167. [[CrossRef](#)]
80. Kakavas, M.; Kyriou, A.; Nikolakopoulos, K.G. Assessment of Freely Available DSMs for Landslide-Rockfall Studies. In Proceedings of the Earth Resources and Environmental Remote Sensing/GIS Applications XI, Edinburgh, UK, 20 September 2020; International Society for Optics and Photonics. Volume 11534, p. 115340R. [[CrossRef](#)]
81. Keijsers, J.G.S.; Schoorl, J.M.; Chang, K.-T.; Chiang, S.-H.; Claessens, L.; Veldkamp, A. Calibration and resolution effects on model performance for predicting shallow landslide locations in Taiwan. *Geomorphology* **2011**, *133*, 168–177. [[CrossRef](#)]
82. Frattini, P.; Crosta, G.; Carrara, A.; Agliardi, F. Assessment of rockfall susceptibility by integrating statistical and physically-based approaches. *Geomorphology* **2008**, *94*, 419–437. [[CrossRef](#)]
83. Booth, A.M.; Roering, J.J.; Perron, J.T. Automated landslide mapping using spectral analysis and high-resolution topographic data: Puget Sound lowlands, Washington, and Portland Hills, Oregon. *Geomorphology* **2009**, *109*, 132–147. [[CrossRef](#)]
84. Ravelle, L.; Allignol, F.; Deline, P.; Gruber, S.; Ravello, M. Rock falls in the Mont Blanc Massif in 2007 and 2008. *Landslides* **2010**, *7*, 493–501. [[CrossRef](#)]
85. Mancini, F.; Ceppi, C.; Ritrovato, G. GIS and statistical analysis for landslide susceptibility mapping in the Daunia area, Italy. *Nat. Hazards Earth Syst. Sci.* **2010**, *10*, 1851–1864. [[CrossRef](#)]
86. Fernández, T.; Irigaray, C.; El Hamdouni, R.; Chacón, J. Methodology for Landslide Susceptibility Mapping by Means of a GIS. Application to the Contraviesa Area (Granada, Spain). *Nat. Hazards* **2003**, *30*, 297–308. [[CrossRef](#)]
87. Bianchini, S.; Solari, L.; Casagli, N. A GIS-Based Procedure for Landslide Intensity Evaluation and Specific Risk Analysis Supported by Persistent Scatterers Interferometry (PSI). *Remote Sens.* **2017**, *9*, 1093. [[CrossRef](#)]
88. Guzzetti, F.; Carrara, A.; Cardinali, M.; Reichenbach, P. Landslide hazard evaluation: A review of current techniques and their application in a multi-scale study, Central Italy. *Geomorphology* **1999**, *31*, 181–216. [[CrossRef](#)]
89. Acosta, E.; Agliardi, F.; Crosta, G.B.; Rios Aragues, S. Regional Rockfall Hazard Assessment in the Benasque Valley (Central Pyrenees) Using a 3D Numerical Approach. In Proceedings of the 4th EGS Plinius Conference—Mediterranean Storms, Mallorca, Spain, 2–4 October 2002; pp. 555–563.
90. Sartori, M.; Baillifard, F.; Jaboyedoff, M.; Rouiller, J.-D. Kinematics of the 1991 Randa rockslides (Valais, Switzerland). *Nat. Hazards Earth Syst. Sci.* **2003**, *3*, 423–433. [[CrossRef](#)]
91. Agliardi, F.; Crosta, G.; Zanchi, A. Structural constraints on deep-seated slope deformation kinematics. *Eng. Geol.* **2001**, *59*, 83–102. [[CrossRef](#)]

92. Thiery, Y.; Sterlacchini, S.; Malet, J.P.; Puissant, A.; Remaître, A.; Maquaire, O. Strategy to Reduce Subjectivity in Landslide Susceptibility Zonation by GIS in Complex Mountainous Environments. In Proceedings of the 7th AGILE Conference on GIScience, Heraklion, Greece, 29 April–1 May 2004; pp. 623–634.
93. Yu, M.; Huang, Y.; Xu, Q.; Guo, P.; Dai, Z. Application of virtual earth in 3D terrain modeling to visual analysis of large-scale geological disasters in mountainous areas. *Environ. Earth Sci.* **2016**, *75*. [[CrossRef](#)]
94. Carrara, A.; Guzzetti, F.; Cardinali, M.; Reichenbach, P. Use of GIS technology in the prediction and monitoring of landslide hazard. *Nat. Hazards* **1999**, *20*, 117–135. [[CrossRef](#)]
95. Nichol, J.; Wong, M.S. Satellite remote sensing for detailed landslide inventories using change detection and image fusion. *Int. J. Remote Sens.* **2005**, *26*, 1913–1926. [[CrossRef](#)]
96. Huang, Y.; Yu, M.; Xu, Q.; Sawada, K.; Moriguchi, S.; Yashima, A.; Liu, C.; Xue, L. InSAR-derived digital elevation models for terrain change analysis of earthquake-triggered flow-like landslides based on ALOS/PALSAR imagery. *Environ. Earth Sci.* **2014**, *73*, 7661–7668. [[CrossRef](#)]
97. Chigira, M.; Wu, X.; Inokuchi, T.; Wang, G. Landslides induced by the 2008 Wenchuan earthquake, Sichuan, China. *Geomorphology* **2010**, *118*, 225–238. [[CrossRef](#)]
98. Abellán, A.; Vilaplana, J.M.; Martínez, J. Application of a long-range Terrestrial Laser Scanner to a detailed rockfall study at Vall de Núria (Eastern Pyrenees, Spain). *Eng. Geol.* **2006**, *88*, 136–148. [[CrossRef](#)]
99. Palma, B.; Parise, M.; Reichenbach, P.; Guzzetti, F. Rockfall hazard assessment along a road in the Sorrento Peninsula, Campania, southern Italy. *Nat. Hazards* **2011**, *61*, 187–201. [[CrossRef](#)]
100. Tarolli, P.; Dalla Fontana, G. Hillslope-to-valley transition morphology: New opportunities from high resolution DTMs. *Geomorphology* **2009**, *113*, 47–56. [[CrossRef](#)]
101. Žabota, B.; Repe, B.; Kopal, M. Influence of digital elevation model resolution on rockfall modelling. *Geomorphology* **2018**. [[CrossRef](#)]
102. Jaboyedoff, M.; Choffet, M.; Derron, M.-H.; Horton, P.; Loye, A.; Longchamp, C.; Mazotti, B.; Michoud, C.; Pedrazzini, A. Preliminary Slope Mass Movement Susceptibility Mapping Using DEM and LiDAR DEM. In *Terrigenous Mass Movements*; Springer: Cham, Switzerland, 2012; pp. 109–170. [[CrossRef](#)]
103. Lan, H.; Derek Martin, C.; Lim, C.H. RockFall analyst: A GIS extension for three-dimensional and spatially distributed rockfall hazard modeling. *Comput. Geosci.* **2007**, *33*, 262–279. [[CrossRef](#)]
104. Nikolakopoulos, K.; Depountis, N.; Vagenas, N.; Kavoura, K.; Vlachaki, E.; Kelasidis, G.; Sabatakakis, N. Rockfall Risk Evaluation Using Geotechnical Survey, Remote Sensing Data, and GIS: A Case Study from Western Greece. In Proceedings of the Third International Conference on Remote Sensing and Geoinformation of the Environment (RSCy2015), Paphos, Cyprus, 19 June 2015. [[CrossRef](#)]
105. Agliardi, F.; Crosta, G.B. High resolution three-dimensional numerical modelling of rockfalls. *Int. J. Rock Mech. Min. Sci.* **2003**, *40*, 455–471. [[CrossRef](#)]
106. Guzzetti, F.; Reichenbach, P.; Wiecek, G.F. Rockfall hazard and risk assessment in the Yosemite Valley, California, USA. *Nat. Hazards Earth Syst. Sci.* **2003**, *3*, 491–503. [[CrossRef](#)]
107. Crosta, G.B.; Agliardi, F. A methodology for physically based rockfall hazard assessment. *Nat. Hazards Earth Syst. Sci.* **2003**, *3*, 407–422. [[CrossRef](#)]
108. Lee, S.; Choi, J.; Woo, I. The effect of spatial resolution on the accuracy of landslide susceptibility mapping: A case study in Boun, Korea. *Geosci. J.* **2004**, *8*, 51–60. [[CrossRef](#)]
109. Aksoy, H.; Ercanoglu, M. Determination of the rockfall source in an urban settlement area by using a rule-based fuzzy evaluation. *Nat. Hazards Earth Syst. Sci.* **2006**, *6*, 941–954. [[CrossRef](#)]
110. Derron, M.-H.; Jaboyedoff, M.; Blikra, L.H. Preliminary assessment of rockslide and rockfall hazards using a DEM (Oppstadhornet, Norway). *Nat. Hazards Earth Syst. Sci.* **2005**, *5*, 285–292. [[CrossRef](#)]
111. Qin, C.-Z.; Bao, L.-L.; Zhu, A.-X.; Wang, R.-X.; Hu, X.-M. Uncertainty due to DEM error in landslide susceptibility mapping. *Int. J. Geogr. Inf. Sci.* **2013**, *27*, 1364–1380. [[CrossRef](#)]
112. Volkwein, A.; Schellenberg, K.; Labiouse, V.; Agliardi, F.; Berger, F.; Bourrier, F.; Dorren, L.K.A.; Gerber, W.; Jaboyedoff, M. Rockfall characterisation and structural protection—A review. *Nat. Hazards Earth Syst. Sci.* **2011**, *11*, 2617–2651. [[CrossRef](#)]
113. Stevens, W.D. RocFall, a Tool for Probabilistic Analysis, Design of Remedial Measures and Prediction of Rockfalls. Master's Thesis, University of Toronto, Toronto, ON, Canada, 1998.
114. Corona, C.; Trappmann, D.; Stoffel, M. Parameterization of rockfall source areas and magnitudes with ecological recorders: When disturbances in trees serve the calibration and validation of simulation runs. *Geomorphology* **2013**, *202*, 33–42. [[CrossRef](#)]
115. Dorren, L.K.A. *Rockyfor3D (v5.0) Revealed—Transparent Description of the Complete 3D Rockfall Model*; EcorisQ Paper: Geneva, Switzerland, 2012.
116. Geostru GeoRock. *User Guide*; Geostru Software: Cosenza, Italy, 2004.
117. Geostru GeoRock. *3D User Guide*; Geostru Software: Cosenza, Italy, 2009.
118. Bühler, Y.; Christen, M.; Glover, J.; Bartelt, P. Significance of Digital Elevation Model Resolution for Numerical Rockfall Simulations. In Proceedings of the 3rd International Symposium Rock Slope Stability C2ROP, Lyon, France, 15–17 November 2016; pp. 15–17.

119. Pack, R.T.; Tarboton, D.G.; Goodwin, C.N. Terrain Stability Mapping with SINMAP, Technical Description and Users Guide for Version 1.00. 1998. Available online: <https://www.semanticscholar.org/paper/Terrain-Stability-Mapping-with-SINMAP%2C-technical-Pack-Tarboton/b55931b905be0d789e6c719e7ba0e56bfbea7d48> (accessed on 8 April 2021).
120. CREALP. *Software for the Analysis of Spatial Distribution of Discontinuities in Cliffs: Mattercliff*; CREALP: Sion, Switzerland, 2003; Available online: <http://www.crealp.ch/> (accessed on 8 April 2021).
121. Jaboyedoff, M.; Baillifard, F.; Philipposian, F.; Rouiller, J.-D. Assessing fracture occurrence using “weighted fracturing density”: A step towards estimating rock instability hazard. *Nat. Hazards Earth Syst. Sci.* **2004**, *4*, 83–93. [[CrossRef](#)]
122. Guzzetti, F.; Crosta, G.; Detti, R.; Agliardi, F. STONE: A computer program for the three-dimensional simulation of rock-falls. *Comput. Geosci.* **2002**, *28*, 1079–1093. [[CrossRef](#)]
123. Scioldo, G. *User Guide ISOMAP & ROTOMAP—3D Surface Modelling and Rockfall Analysis*; Geo&Soft International: Torino, Italy, 2006.
124. Jaboyedoff, M.; Metzger, R.; Oppikofer, T.; Couture, R.; Derron, M.H.; Locat, J.; Turmel, D. New Insight Techniques to Analyze Rock-Slope Relief Using DEM and 3D Imaging Cloud Points: COLTOP-3D Software. In Proceedings of the 1st Canada-US Rock Mechanics Symposium, Vancouver, BC, Canada, 27–31 May 2007. American Rock Mechanics Association.
125. Jaboyedoff, M.; Labiouse, V. Preliminary Assessment of Rockfall Hazard Based on GIS Data. In Proceedings of the 10th ISRM Congress, Sandton, South Africa, 8–12 September 2003; International Society for Rock Mechanics and Rock Engineering: Lisbon, Portugal.
126. Jaboyedoff, M.; Labiouse, V. Technical Note: Preliminary estimation of rockfall runout zones. *Nat. Hazards Earth Syst. Sci.* **2011**, *11*, 819–828. [[CrossRef](#)]
127. International Institute for Aerospace Survey and Earth Sciences. *ILWIS 2.2 for Windows, the Integral Land and Water Information System: Reference Guide*; ILWIS Development ITC: Enschede, The Netherlands, 1999.
128. Carrara, A.; Cardinali, M.; Detti, R.; Guzzetti, F.; Pasqui, V.; Reichenbach, P. GIS techniques and statistical models in evaluating landslide hazard. *Int. J. Rock Mech. Min. Sci. Geomech. Abstr.* **1991**, *29*, A102. [[CrossRef](#)]
129. Claessens, L.; Heuvelink, G.B.M.; Schoorl, J.M.; Veldkamp, A. DEM resolution effects on shallow landslide hazard and soil redistribution modelling. *Earth Surf. Proc. Landf.* **2005**, *30*, 461–477. [[CrossRef](#)]
130. McLean, A. Landslide risk assessment using digital elevation models. *Can. Geotech. J.* **2011**. [[CrossRef](#)]
131. Marquínez, J.; Menéndez Duarte, R.; Farias, P.; Jiménez Sánchez, M. Predictive GIS-Based Model of Rockfall Activity in Mountain Cliffs. *Nat. Hazards* **2003**, *30*, 341–360. [[CrossRef](#)]
132. Dorren, L.K.A. A review of rockfall mechanics and modelling approaches. *Prog. Phys. Geogr.* **2003**, *27*, 69–87. [[CrossRef](#)]
133. Crosta, G.B.; Frattini, P.; Valbuzzi, E.; De Blasio, F.V. Introducing a New Inventory of Large Martian Landslides. *Earth Space Sci.* **2008**, *5*, 89–119. [[CrossRef](#)]
134. Kalapodis, N.; Kampas, G.; Ktenidou, O.-J. A review towards the design of extraterrestrial structures: From regolith to human outposts. *Acta Astronautica* **2020**. [[CrossRef](#)]
135. Leonovich, A.K.; Gromov, V.V.; Dmitriev, A.D.; Lozhkin, V.A.; Pavlov, P.S.; Rybakov, A.V. Physical and mechanical properties of lunar soil sample in nitrogen medium: Research results. *Lunnyi Grunt iz Morya Izobiliya* **1974**, 563–570.